AI 1978

CONF-780857--1

Prepared for presentation at the International Conference on "Dynamical Properties of Heavy-Ion Reactions", Johannesburg, South Africa, Aug. 1-3, 1978

MASTER

Resonances and Backward-Angle Scattering

NOTICE
This report was prepared as an account of work sponsored by the United States Government. Neither the United States nor the United States Department of Energy, nor any of their employees, nor any of their contractors, subcontractors, or their employees, makes any warranty, express or implied, or assumes any legal liability or responsibility for the accuracy, completeness or usefulness of any information, apparatus, product or process disclosed, or represents that its use would not infringe privately owned rights.

R.G. Stokstad

Gesellschaft für Schwerionenforschung
6100 Darmstadt, Germany
and
Oak Ridge National Laboratory[x]
Oak Ridge, Tennessee, 37830, U.S.A.

Abstract

The strong enhancement of elastic scattering at large angles observed for systems such as $\alpha+^{40}Ca$ and recently for $^{12}C+^{28}Si$ and $^{16}O+^{28}Si$ has been interpreted in terms of entrance channel resonances having a quasi-molecular character. Alternative explanations in terms of potential scattering have also been presented. An overview is given of the experimental data and their interpretations. A consistent procedure for the evaluation of the experimental data is discussed.

DISTRIBUTION OF THIS DOCUMENT IS UNLIMITED

[x]permanent address, work supported by the Department of Energy

1. Introduction

The reactions of light heavy-ions ($A \lesssim 40$) very often show a pronounced structure in their dependence on bombarding energy and on scattering angle. The character of this structure can itself vary depending on the projectile-target combination, the energy above the Coulomb barrier, and the reaction channel under observation. Many of the structures suggest a resonant behaviour while others are characteristic of potential scattering, and frequently it can be difficult to distinguish between them.

Resonances are usually classified as compound nuclear fluctuations, intermediate structures or entrance channel resonances. These classifications reflect the relative number of degrees of freedom (many, a few, and one, respectively) involved in producing a given structure or bump in the cross section. The study of compound fluctuations has matured; the topic of intermediate structures (quasi-molecular phenomena) is discussed extensively in the proceedings of the Hvar Conference [Cin 77] last year. Entrance channel resonances also have a long history which I cannot attempt to recount. Rather, I want to focus on a particular aspect of this structure, viz. anomalously large scattering at backward angles, an area which has experienced a rapid development within the last two years. In the case of α-particle scattering, where the effect has been known for a long time and extensive data are available, the most recent developments are in the interpretation of the data. The observation of a back-angle anomaly (BAA) in systems such as $^{16}O+^{28}Si$ and $^{12}C+^{28}Si$ has been so recent that this area is still in its infancy. However, interesting parallels in the two areas are already evident.

Since time and space limitations allow only an overview of the subject, the list of references will not be complete. Also, experiments on inelastic scattering, transfer reactions and fusion unfortunately could not be covered, even though many interesting results have been obtained recently.

Recent review talks by Siemssen [Sie 77] and by Eberhard [Ebe 78] have been helpful in the preparation of this article.

After considering selected examples of the experimental data and their analyses in the next section, section III will delve in more detail into the evidence for resonant and non-resonant scattering. Semi-classical methods will also be considered there. The last section looks into the future and suggests a consistent procedure for evaluating the experimental data.

2. Overviews of experimental results and analysis.

2.1 α-particle scattering

The BAA was first seen in the scattering of α-particles, a nuclear species which should also be classified as a "heavy-ion" in the sense that it is strongly absorbed. Fig. 1, taken from the work of Löhner et. al. [Löh 78] illustrates the salient features. α-scattering from the isotopes of ^{40}Ca and ^{44}Ca is similar in the angular region forward of 60° and is markedly different in the back-angle region, $\theta > 120^{\circ}$. At energies $\gtrsim$60 MeV both targets yield angular distributions similar at all angles. In the energy region where the BAA occurs, a $P_J^2(\cos\theta)$ pattern emerges, with J close to the grazing angular momentum, l_{gr}. The angular momenta and energies at which these patterns emerge form a rotational band (S to 72) as shown in Fig. 2 [Löh 78]. The effect is strongly isotope dependent, i. e., targets of ^{36}Ar, ^{39}K and ^{40}Ca exhibit a BAA whereas ^{40}Ar, ^{41}K, ^{42,44}Ca do not [Sto 72]. Ni targets and heavier nuclei show no enhancement [Tro 74, Wit 75]. Since the type of back-angle scattering observed with targets such as ^{42,44}Ca could be described by a standard four-parameter Woods-Saxon optical potential, their behaviour was taken as the norm against which the anomalous cases were identified.

Despite an extensive body of experimental data, a satisfactory understanding of the BAA has not yet emerged. Two lines of thought have developed which we will sketch briefly before moving on to the recent experimental results for heavier projectiles. One school, e.g., [Sto 72, Sto 72b, Löh 78] maintains that a standard optical model (standard now in the sense that the potentials do not vary rapidly with target nucleon number) should be used to describe the diffractive scattering dominant at forward angles and present also,

but presumably much smaller, at backward angles. To this should then be added an additional resonance term (often parametrised as a Regge-pole [McV 71] which describes the BAA. Other workers try to find an explanation of the anomaly in terms of the potentials alone [Mic 77, Gub 78, Del 78]. To this end, variations in the shapes of the potentials are explored, and the isotope effect is reflected mainly in a variation of the imaginary potential.

2.2 ^{12}C and ^{16}O scattering

The elastic scattering of ^{12}C and ^{16}O by light targets has received new emphasis, primarily through a series of recent measurements on the system $^{16}O+^{28}Si$ [Cra 76, Bra 77, Bar 78]. The experimental data of Cramer et. al. [Cra 76] are shown in Fig. 3. With the exception of the four energies at E_{lab} = 50 - 66 MeV, these data in the forward hemisphere are well reproduced by the optical model calculations [Cra 76, Sat 77] shown in the figure. At these four energies, the optical model does not reproduce the oscillations appearing in the data, although the general trend is correct. Both potentials used in the calculations are similar in the surface region and give nearly identical cross sections, at least for the forward angles shown here. At 55 MeV, the potential called E 18 (a shallow real potential [Cra 76]) predicts a nearly monotonic decrease in the cross section for scattering angles extending out to 180°. Thus, it predicts the absence of a back-angle enhancement. Since it reproduces the scattering reasonably well over a large energy region, it may be taken as a "background" potential to account for the diffractive scattering at forward angles.

Of course, it was realized that the E 18 potential does not predict a BAA only after the experiments of Braun-Munzinger et.al. [Bra 77] showed that such an enhancement indeed exists. (Fig. 4). The ratio $d\sigma/d\sigma_{Ruth}$ at 180° is 10^{-2} whereas for $\alpha+^{40}Ca$ this ratio can be as large as 1. Relative to the prediction of the strongly absorbing E18 potential, however, the back-angle rise represents a strong enhancement. A P_J^2 angular distribution is observed.

Measurements for $^{12}C+^{28}Si$ at forward angles [Che 77] and at angles from 120° - 180° [Clo 78] reveal a situation very similar to that just described for $^{16}O+^{28}Si$. In fig. 5 one notes that a P_J^2 pattern appears at some energies while it is absent at others. The overall back-angle enhancement is present at all energies. Fig. 6 shows an excitation function measured [Bar 78] at $\theta = 175^{o}$ - 180° for $^{16}O+^{28}Si$; similar structure is observed for $^{12}C+^{28}Si$ [Clo 78]. There is also an isotope effect - Clover et. al. [Clo 78] report that cross sections for $^{13}C+^{28}Si$ and $^{9}Be+^{28}Si$ at back angles generally do not show strong oscillations and that the elastic cross sections are surpressed by an order-of-magnitude compared with the $^{12}C+^{28}Si$ system. This summarises the main experimental observations for the back-angle scattering of ^{12}C and ^{16}O from ^{28}Si.[x]

---

[x]We should note that there is another class of experiments in which a back-angle enhancement has been known for a long time, e.g. $^{12}C+^{13}C$, $^{12}C+^{16}O$, etc. This has not been termed anomalous because the difference in mass between projectile and target is sufficiently small that the scattering at large angles can be explained by the transfer of a nucleon, or cluster of nucleons [Von 70]. However, nucleon exchange is one of the ways to explain these data, l-dependent absorption being another [Cha 70].

It is clear that the results of α-particle and heavy-ion scattering have much in common. This is true also of their interpretation; indeed two schools of thought appear to be developing. Braun-Munzinger et. al. [Bra 77] incorporated a Regge-pole term in the background S-matrix given by the E-18 potential (see Fig. 4). Other authors [Den 77, Che 77, Lee 77, Den 78, Shk 78] have sought to explain these data without explicitly introducing resonant mechanisms into the S-matrix directly, but by modifying the potentials themselves.

3. Interpretation

The main features of the experimental results for the BAA have

been illustrated and their divergent interpretations mentioned. We now want to discuss these interpretations in more detail, exploiting where possible the similar nature of the α-particle and ^{12}C or ^{16}O induced reactions.

3.1 Resonances or molecular phenomena

We begin by suggesting reasonable requirements for the interpretation of the above data in terms of resonant molecular phenomena.

i) The structure of the molecule in the compound system should be simple. Thus, we envision a system of two spatially defined clusters rotating with good angular momentum and parity.

ii) The moment of inertia should be reasonably constant such that a rotational band emerges.

iii) The molecule should rotate through an angle $\theta \gtrsim 2\pi$ before it decays. Or, the lifetime of the state formed in a heavy-ion collision should substantially exceed some characteristic time corresponding, for example to the contact time of a normal classical trajectory. Otherwise, all collisions can be said to form a nuclear molecule.

3.1.1 $\alpha + {}^{40}Ca$

Points i) and ii) above seem to be well satisfied. That the points in Fig. 2 lie on a straight line indicates a constant moment of inertia. (Unfortunately, the experimental errors on the energies at which the P_J^2 structures occur are not given). The value of the moment- of-inertia, indicated by the slope of the line corresponds to an $\alpha + {}^{40}Ca$ rotor, which is substantially larger than that of a spherical ^{44}Ti nucleus. Microscopic theoretical calculations based on cluster-model wave functions also lend partial support to point i). Although the use of the cluster-model presumes the existence of clusters, it is reassuring that, even for $l = 0$, a minimum in the potential energy of the system is attained for a separation between the centers corresponding to an $\alpha + {}^{40}Ca$ rotor [Fri 75, Fri 75a]. Point iii) is difficult. To examine it

means that the widths for the cluster structure must be known. Dynamical predictions made with the resonating group method (RGM) are shown in fig. 7b [Fri 75, Fri 75a]. The energy of the resonance is the value at which the derivative of the phase shift, $\frac{d\delta_\ell}{dE}$, has a maximum and the width is given by

$$\Gamma = 2\left\{ \left(\frac{d\delta_\ell}{dE}\right)_{E=E_r} \right\}^{-1}$$

The agreement with the measured resonance energies is good. The predicted width for the 1^- state at E_{cm} = 6.6 MeV is 120 keV, whereas the measured widths are Γ_α = 31 keV and Γ_{tot} = 51 keV [Fre 76]. Considering the fact that this level lies near the Coulomb barrier and the width is thus sensitive to penetrability effects, the agreement here is quite good. This 1^- level, by virtue of its relatively large α-width, its location on the rotational band line shown in Fig. 2, and its long lifetime, satisfies all our above criteria for a nuclear molecular resonance. (The experimental and theoretical effort connected with establishing quantitatively the properties of this level was considerable and represents an admirable piece of work.) The widths of the levels with spins 8-15 have not been measured; in this respect, fitting the data with a resonance parametrized in energy as well as with the more frequently used and simpler Regge-pole expression could be valuable. If the experimental widths are of the order of half the spacing between adjacent levels in the band, then experiment and theory are in fair agreement for the 8^+ and 9^- levels. However, the theory overestimates the widths of the higher spin levels, and in fact predicts life times too short by factors of 2-4 to be consistent with the time required for the α-^{40}Ca system to make one rotation. The rough upper limits we have placed on the experimental widths indicate lifetimes equal to or longer than a collision time, and rotations $\theta \gtrsim \pi$. Clearly, it would be of great value to have a more precise estimate of the experimental widths.

The RGM calculations predict that the band terminates with l=15, since for higher spins the cluster is no longer quasi-bound. This is in qualitative agreement with experiment since the angular distributions are no longer anomalous at energies above $\sim$45 MeV c.m.

Fig. 2 predicts the approximate locations of the other members of the band with l = 2-7. The observation of these levels would be of great significance for the molecular interpretation. An experimental search for these levels is the subject of a contribution to this conference [Sel 78]. Although the spins have not yet been determined, candidates for the members of the band are reported [Sel 78].

The arguments for a molecular interpretation of the BAA in $\alpha+^{40}Ca$ are persuasive. We consider the $^{12}C+^{28}Si$ and $^{16}O+^{28}Si$ systems next.

3.1.2 $^{12}C+^{28}Si$, $^{16}O+^{28}Si$

The experimental data in this case are not as complete as for $\alpha+^{40}Ca$. While the respective systems have in common the fact that the J-values deduced from the angular distributions are generally within several units of the grazing angular momentum, there are two important differences. One is that the angular momenta do not indicate as constant a moment-of-inertia [Clo 78, Clo 78a, Bar 78]. The other, and more important difference, is that the energy spacing between the structures is too broad for a rotational band with all angular momenta present. This is shown in Fig. 6 for $^{16}O+^{12}C$ and in Fig. 8 for $^{12}C+^{28}Si$ (Bar 78). Approximately every other l-value is missing at the higher energies. The difficulties of interpreting the results for the latter reaction in terms of a normal rotational band have been noted by Clover et. al. [Clo 78]. Barrette et. al. [Bar 78] have suggested a possible explanation for this interms of series of rotational bands with different principle quantum numbers. A given number of a band becomes visible only if it lies near the grazing "window". However, it seems certain that the strength and position of such resonances would be affected drastically by the inclusion of absorption, the calculation [Bar 78] having been done with a deep real potential well and no absorption.

The parametrisation of the S-matrix in terms of a Regge-pole plus background [McV 71] has been examined in general by Tamura and Wolter [Tam 72] and recently by Takamesa and Tamura [Tak 78]

for the $^{16}O+^{28}Si$ reaction in particular. They considered the S-matrices from a variety of potentials and suggest that a one-pole-plus-background model may not be the optimum approach for this reaction. For example, the E 18 potential itself (used by Braun-Munzinger et. al. for the background) already produces a pole term which results in a destructive interference at large angles. [Tak 78]. In any case, a Regge-pole such as has been introduced to parametrise the back-angle enhancement still leaves us with the question as to the physical process causing it. In a contribution to this conference, Lipperheide et. al. discuss the inverse problem of deriving the potential from a given background plus Regge-pole. This result is that the imaginary part of the potential is pushed inward, leaving the surface region more transparent [Lip 78] (Why some systems show transparency and others not is another fundamental question).

The energy dependence of the BAA is known only over a very limited region. It is interesting to speculate whether the "band" will terminate and the anomaly disappear at some higher energy. An inspection of the forward-angle data in Fig. 3 suggests that the enhancement will be reduced at energies above 50 MeV c.m. ($E^{16}_{O} \sim 80\ MeV_{lab}$).

This discussion of the molecular interpretation of the data is concluded with some qualitative remarks on the excitation function shown in Fig. 8 [Bar 78]. The gross structures shown there are reminiscent of those seen in $^{16}O+^{16}O$. There is a finer structure also which indicates degrees of freedom more complicated than those of the entrance channel above. Fig. 9, taken from Könnecke et. al. [Kön 77] is a schematic interpretation of such phenomena in terms of the coupling of broadly spaced states in the entrance channel to intermediate structures. The latter have a longer lifetime and correspond to a potential which has evolved from that given by a sudden approximation to a potential corresponding to an adiabatic limit. Thus, the spacing of the intermediate states is smaller. The question is whether the fine structures in Fig. 8 represent the averaging spacing of resolved ($\Gamma/D \lesssim 1$) intermediate resonances, or correspond to the average width of very dense, strongly

overlapping resonances ($\Gamma/D \gg 1$). In the former case, a theoretical prediction of the structure shown is in principle possible, e.g. by the double resonance model [Kön 77]. In the latter extreme limit a statistical treatment of these structures is necessary. Of course, the physical situation can lie anywhere between these two extremes. Hauser-Feshbach calculations such as done by Shapira et. al. [Sha 74] for $^{12}C+^{12}C$ might help determine the origin of these fine structures.

3.2 Potential scattering

A different and equally intensively pursued approach to understanding the anomalous back angle distributions is to reproduce (if possible) all the features of the angular distributions in terms of the scattering from a complex, local optical model potential. Our requirement for this interpretation is that the properties of this potential vary smoothly with bombarding energy. To the extent that resonant phenomena are present they may be reflected in the shape of the potential which has been adjusted to fit the data. Assuming our requirement above can be satisfied, the optical model potential is then a phenomenological parametrisation of the data, from which has to be gleaned the underlying physics. Semiclassical methods which can relate the properties of the potential directly to the characteristics of the angular distribution are invaluable in this respect.

3.2.1 $\alpha + {}^{40}Ca$

The first step in finding potentials which, by themselves, result in a back-angle enhancement, was to reduce the strength of the imaginary potential in the region of the grazing partial wave [Ebe 70]. Although this was accomplished initially by using an l-dependent imaginary potential [Cha 70] similar effects have been achieved by reducing the diffusivity of the imaginary potential [Gob 73]. The result is that the projectile can now "feel" the inner, attractive region of the nuclear potential. Importantly, for α-nucleus scattering at not too high energies, the total real potential has a pocket.

The second step has occurred rather recently and concerns our requirement that the energy dependence of the

potentials with a form factor $\{1 + \exp(\frac{r-R}{r_a})\}^{-\nu}$ were applied by Michel and Vanderpoorten (Mic 77) to α-scattering from ^{40}Ca at E_{lab} = 20 - 50 MeV.

The value of ν was found to be 2.65. (Thus, the potential is similar to a Woods-Saxon squared (WS2) [Gd 75]. Remarkably, the features of the experimental data in the region 20-50 MeV could then be accounted for with this potential, allowing only a linear increase of the imaginary radius with bombarding energy. Very similar results have been obtained also by Gubler et. al., who measured α-scattering from ^{40}Ca at 21 energies in the region 26-47 MeV and analyzed them both with a folding model potential and the "ν = 2.65" form factor [Gub 78]. Their results are shown in Figs. 10 and 11. The normalizations of the real and imaginary potentials were allowed to vary at each energy. The resultant values, as shown in fig. 11 for the folding potential are seen to vary smoothly and nearly linearly with energy. Finally, the Louvain-Zagreb-Mons-Krackow-Munich collaboration [Del 78] have analyzed cross sections for $^{40}Ca + \alpha$, E = 40 - 62 MeV and $^{44}Ca + \alpha$, E = 40 - 58 MeV using WS2 from factors with independent real and imaginary geometries. With fixed geometry and linear variation in the potential strengths, remarkably good fits to the data are obtained. The real potentials for ^{40}Ca and ^{44}Ca are very similar, whereas the imaginary potentials differ with the larger absorption associated with ^{44}Ca. The problem of discreet ambiguities in the real potential is avoided by using a potential which also fits α-scattering at higher energies. At these energies, discreet ambiguities are removed by the cross sections at angles beyond the nuclear rainbow [Gol 74].

The significance of the WS2 potential is twofold. Since it gives a much improved fit to the experimental data over a wide energy range, its shape, therefore, more nearly represents the shape of the effective local optical potential to be used in the Schrödinger equation. Second, its shape is justified from a theoretical standpoint by the folding model. Figure 12 compares the ν=2.65 potential of Michel et. al. with that of the double folding model [Lov 78]. It is worth noting that a recent folding model analysis of $^{12}C+^{12}C$ scattering a high energies and at large angles ($\theta_{c.m.} \sim 60^{\circ} - 90^{\circ}$,

since the particles are identical) has indicated the need for a deep potential [Wie 76].

3.2.2 $^{12}C+^{28}Si$ and $^{16}O+^{28}Si$

Optical potentials which reproduce the back-angle enhancement in the $^{16}O+^{28}Si$ system have been explored by Denhard and collaborators [Den 77, Den 78, Shk 78]. The differences between the shallow, strongly absorbing potential E 18 (which shows no back angle enhancement) and the potential which does, are illustrated in Figs. 13a and 13b. They introduced a more attractive nuclear potential, such that a pocket is produced, and a weaker absorption in the surface region. The l-dependent potential shown in Fig. 13a produces an angular distribution very similar (although not identical to that of the E 18 potential + Regge-pole [Bra 77]. The corresponding S-matrices, however, are quite different, as is shown in Fig. 14 [Den 77, Shk 78]. The one potential produces an S-matrix with a sharper transition in l from complete absorption while the effect of the Regge-pole is to produce a kink extending over three l-values. This ambiguity in the S-matrix at this particular energy illustrates a common problem in the analysis of complex-particle scattering and points to the need for angular distributions over a wide range of energies.

The 180° excitation function for $^{16}O+^{28}Si$ [Bar 78] is shown in Fig. 6. As indicated in the figure, the spacing of the broad structures is too great to allow identification of the maxima with successive values of angular momenta (which was possible for $\alpha + {}^{40}Ca$). This precludes an interpretation in terms of a single rotational band and would indicate, as already noted, that the individual structures must correspond to members of bands with different

principle quantum numbers [Bar 78]. Lee and Chan [Lee 78] employed a proximity-type potential and were able, roughly, to reproduce the spacings of the structures shown in Fig. 6. Denhard et. al. [Den 78] have shown that the structures can be reproduced remarkably well by the addition of a small parity dependent term to the optical potential. Theoretical justifications for such a term have been presented [Den 78]. The fit shown in Fig. 6 to the excitation function is surprisingly good; but a comparison with full angular distributions, of course, would pose a more severe test.

We have seen that the experimental data available so far are well reproduced by certain types of optical model potentials. We would like to know why this is so.

3.2.3 Semi-classical analyses of potential scattering

It is difficult to discover the physics governing the connection between the input and output of an optical model calculation. Numerical solutions of the Schrödinger equation have the advantage of being exact but they are not physically transparent.

Semiclassical methods have recently made significant contributions to our understanding of the relationship between optical model potentials and the resultant angular distributions. They also allow an insight into the nature of the resonances produced by potential scattering.

Brink and Takigawa [Bri 77] have derived analytic formulas in the WKB approximation for the case of a complex Woods-Saxon potential having three turning points. Such a potential, shown for the scattering of 29 MeV α-particles with $l = 15$ by ^{40}Ca is shown in Fig. 15. The angular distribution is determined by three "action" integrals of the type

corresponding to the three regions indicated in Fig. 15. The separation variable r is extended into the complex plane.

The scattering amplitude or S-matrix element can be divided

into two components $S = S_B + S_I$ where the barrier amplitude S_B is determined mainly by the integral in region 1 and the inner amplitude by region 3. For other ways of decomposing the S-matrix into two interfering amplitudes, see [Dou 77]. If E is very close to V_B, then the integral in region 2 (i.e. the barrier penetration) contributes to both S_B and to S_I. The value of S_B is rather insensitive to the strength of the imaginary potential W_o whereas S_I varys strongly. This is illustrated in fig. 16 where S_I and S_B (η_I and η_B in Brink's notation) are shown as functions of ℓ for two values of the imaginary potential. The larger value of W corresponds to the scattering of $\alpha + {}^{44}Ca$, i.e. to the case with no back-angle anomaly. The barrier and inner amplitudes each very smoothly with l, but their coherent summation results in an odd-even oscillation in an otherwise smooth variation of the total amplitude. This is shown in Fig. 17. The magnitude of S for the low l values ($l \lesssim 7$) and the strength of this odd-even perturbation in the transition region l = 8-13 depends on the size of S_I and hence on the strength of W in region 3. Fig. 18 shows angular distributions calculated for each of the amplitudes separately, where $\sigma_B(\theta) = |f_B(\theta)|^2$, $\sigma_I(\theta) = |f_I(\theta)|^2$, and $\sigma(\theta) = |f_B(\theta) + f_I(\theta)|^2$

(The Coulomb amplitude f_c is contained only in f_B). Thus, for a potential of the type shown in Fig. 15 which has a barrier, the rise at back angles is caused by the incomplete absorption and consequent reflection of the lower partial curves ($l \lesssim l_{gr}$) by the inner barrier, whereas the forward angle scattering is dominated by reflection from the outer barrier. The intermediate angle region contains interfering contributions from both. When the absorption is increased, the back-angle contribution from $f_I(\theta)$ is reduced and a "normal" angular distribution results. In the case of the E 18 potential of Cramer et. al. (see Fig. 13b), the absence of a pocket results in a single, smoothly varying scattering amplitude and the strong imaginary potential in the interior surpresses any contribution from the lower partial waves.

The above semiclassical treatment has the advantage that it enables us to quantify three levels of absorption and to connect

them with characteristic features of the data.

(i) Complete absorption, in which case the inner amplitude S_I is absent. This corresponds to what is usually termed "strong absorption" in the literature and is defined by

$$|S_I| \approx \exp(-2\mu R W_0 / \hbar^2 K) \ll 1$$

(Eq. 4.8 of [Bri 77]). $\ddot{R}$ is an effective radius of the imaginary potential, W_0 its depth and K is the wave number at r = 0 for ℓ = 0. Angular distributions of the type shown by the dashed curve in Fig. 4 result. Only the tail of the potential is of any consequence.

(ii) Moderate absorption, in which $|S_I|$ is sufficiently large to cause a rise at back angles, but the absorption is still sufficient to damp quasibound resonances in the potential well. This condition is given by

$$W(R_B) \gtrsim 0.5 \left(\hbar^2 V_B'' / \mu\right)^{1/2}$$

(Eq. 3.22 of [Bri 77]) where W and the second derivative of V are evaluated at the position of the barrier R_B. Potentials in this classification are often called surface transparent. (Brink and Takigawa, however, call them strongly absorbing.)

(iii) Weak absorption. Defined by the converse of the above inequality, such potentials can support quasibound resonances in the pocket of the potential well. At the resonance energies, multiple reflection occurs in the pocket and the value of S_B is strongly enhanced. Such phenomena are molecular resonances; they satisfy not only the requirements suggested earlier for molecular phenomena, but also are resonances in the real sense of the Bohr-Sommerfeld quantization rule. As an example, a recent semiclassical analysis of an l-dependent potential describing $^{16}O+^{12}C$ scattering [Tak 78a] has revealed such a long-lived resonance.

Takigawa and Lee [Tak 77] have analyzed in detail the potential for $\alpha+^{40}Ca$ shown in Fig. 12. These results may be summarized as

follows. The classical deflection function for waves scattered from the inner barrier passes smoothly through $-\pi$ for an l-value near grazing, which produces a characteristic rise and interference pattern in the cross section near 180°. (The optical analog is called "glory" scattering [For 59]). As the bombarding energy is varied, the glory angular momentum l_{gl} varies as $E \propto l_{gl}(l_{gl}+1)$ and produces a series of characteristic oscillations, $P^2_{l_{gl}}$ at back angles. Interference of the barrier amplitude and the inner (glory) amplitude is responsible for the structure in the intermediate angle region. (This intermediate angle region is supposed to offer a possibility of distinguishing between a Regge-pole plus background description and the glory scattering). The glory scattering disappears at high energies because the pocket in the total potential disappears and the absorption increases. The isotope effect is caused by different absorptive strengths for different targets.

A semiclassical analysis by Lee [Lee 78] of the potentials shown in Fig. 13a for $^{16}O+^{28}Si$ also shows that the back-angle rise arises from the scattering by the inner barrier, although in this case the potential is not sufficiently attractive to produce a glory effect. The most negative scattering angle is $\theta \sim -\pi/2$.

In summary, deep real nuclear potentials which produce a pocket and moderate absorption in the surface region reproduce the data remarkably well. The energy dependence of these potentials (for α-scattering) is smooth. Semiclassical analysis of these potentials show that the back angle rise results from a single, as opposed to a multiple reflection of the wave reaching the inner barrier.

4. Comments and outlook

We have discussed the interpretations and opinions of both schools and, of course, we would like to know which school is right. We can sympathize with the frustration expressed by Lucy in Fig. 19. However Linus' reply clearly will not do - nuclear reactions are far too complex and interesting for that. Most likely there is truth in

both ways of understanding the experimental data. For example, the molecular resonance may be appropriate at low energies, the potential description at higher energies. The two descriptions might well merge in an intermediate energy region. Indeed, we note that for $l \gtrsim 8$, the classical angles of rotation, deduced from the predicted [Fri 75] lifetime for cluster states in $\alpha + {}^{40}Ca$, are comparable to the classical deflection angles [Tak 77] for the wave scattered from the inner barrier of the potential.

We conclude with a discussion of a consistent procedure for interpreting the data, and some speculation on how this field may develop in the near future. Let us begin the argument in the region of high bombarding energy where the anomalies or structures attributed to molecular phenomena are absent. In this region, the potential description is correct by default. Here we should establish the basic character of the real nuclear potential (e.g. shallow or deep for the case of heavy ions, Woods-Saxon or folding model for the α-scattering). Hopefully this energy region will allow the resolution of discrete ambiguities in the potential for heavier ions (e.g. ${}^{12}C$, ${}^{16}O$) as appears to be possible for α-particles. (The new generation of heavy-ion accelerators now under construction may be essential for this). Precise measurements over a wide angular region will certainly be necessary.

To proceed further in our argument, we have to make a basic assumption about the nature of the phenomenological local optical potential we have just determined. We must assume that this potential has a smooth, analytic continuation to lower energies. This assumption could be tested theoretically through studies of the energy dependence of effects due to non-locality, anti-symmetrization exchange interaction, etc. Experimental data at progressively lower energies would be then examined and the smoothly varying parameters of this phenomenological potential determined, (see [Del 78])[x].

---

[x] (If this procedure does not yield smoothly varying parameters, this will be an indication that other processes are present, e.g. non-potential resonances, and explicit resonant terms will have to be added in order to maintain a well-behaved optical potential.

Semiclassical analyses of this empirical potential over a wide range of energies can then be used to establish the nature of the physical processes underlying the scattering. This procedure will have the advantage that precise definitions are available for various physical processes such as resonance, orbiting, refraction, diffraction, rainbow scattering, etc. The effect of absorption on these processes is also taken into account this way. It seems likely, that at energies closer to the Coulomb barrier where the absorption decreases, molecular resonances will also be idendified in such an analysis (for example, the ℓ^- state at 6.6 MeV in $\alpha+{}^{40}Ca$). (The likelihood that the molecular resonances will be fragmented over the intermediate states must be recognized, however [Fes 76]. See also the contribution to this conference by Cole and Toepffer.)

Since the isotope effect in this procedure is incorporated through an ad hoc variation of the imaginary potential, the origins and effects of absorption in the surface region need to receive much more experimental and theoretical work. In the former case, this means measuring the strengths of the other inelastic reaction channels, even if with poor resolution. It is probable that the dependence of heavy-ion reactions on microscopic variables is reflected much more strongly in the absorptive potential than in the real potential. In this way progress toward removing the ad hoc nature of the absorptive potential and toward understanding the origin of surface transparency will be made; this is something of importance for both schools of thought.

In the future we expect that further measurements at low energies will uncover the other low spin members of the $\alpha+{}^{40}Ca$ band and that additional measurements at higher energies will aid in mapping a smooth dependence of the real and imaginary potentials. For the heavier projectiles, our knowledge of the backward angle enhancement will be extended over a greater region of energy - the termination of the enhancement will probably be observed. Further measurements on a variety of systems will establish the isotope effect. Cross bombardments, as for example were made by Vandenbosch et. al. for ${}^{12}C+{}^{20}Ne$ and ${}^{16}O+{}^{16}O$ [Van 74], will help isolate the role of the

entrance channel and probe the nature of absorption. It promises to be an exciting time.

Acknowledgement

This manuscript was prepared at the Gesellschaft für Schwerionenforschung. It is a pleasure to acknowledge the stimulating atmosphere there, and in particular, the hospitality of Drs. A. Gobbi and R. Bock.

References

[Bal 75] A.J. Baltz, et.al. Phys. Rev. C 12, 136 (1975)

[Bar 78] J. Barrette, et.al. Phys. Rev. Letters 40,445 (1978)

[Bra 77] P. Braun-Munzinger, et.al. Phys. Rev. Letters 38,944 (1977)

[Bri 77] D.M. Brink and N. Takigawa, Nucl. Phys. A 279,159 (1977)

[Cha 70] R.A. Chatwin, et.al., Phys. Rev. C 1,795 (1970)

[Che 77] C.M. Cheng, et.al., Phys. Letters 71 B,304 (1977)

[Cin 77] Proc. Int. Conf. on Resonances in Heavy-Ion Reactions Hvar, Yugoslavia (1977)
N. Cindro, Ed. North Holland Pub. Co, 1978

[Clo 78] M.R. Clover, et.al., Phys. Rev. Letters 40,1008 (1978)

[Clo 78a] M.R. Clover, et.al., Proc. 3rd International Conf. on Clastering Aspects of Nuclear Structure, Winnipeg (Canada) 1978

[Col 78] B.T. Cole and C. Toepffer, Contribution No 31 to this conference

[Cra 76] .G. Cramer, et.al., Phys. Rev. C 14, 2158 (1976)

[Del 78] Th. Delbar,et.al., The Louvain-Zagreb-Mons-Krakow-Munich Collaboration; Preprint IPC-N-78o1 (Louvain) 1978; To appear in Phys. Rev. C

[Den 77] D. Denhard, Proc. Symposium on Heavy-Ion Elastic Scattering, Rochester, October 1977, R.M. DeVries, Ed.

[Den 78] D. Denhard, et.al., Phys. Rev. Letters 40, 1549 (1978)

[Dou 77] H. Doubre and C. Marty in Proc. Int. Conf. on Resonances in Heavy-Ion Reactions, Hvar, (1977) p 291. Ed. N. Cindro

[Ebe 70] K.A. Eberhard, Phys. Letters 33 B, 343 (1970)

[Ebe 78] K.A. Eberhard, Proc. Int. School on Nucl. Phys., Zakopane (Poland), 1978

[Fes 76] H. Feshbach, J. Physique 37 C-5 177 (1976)

[Fre 76] D. Frekers, et.al., Z. Physik A 276, 317 (1976)

[Fri 75] H. Friedrich, et.al., Phys. Letters 55 B, 345 (1975)

[Fri 75a] K. Friedrich and K. Langanke, Nucl. Phys. A 252, 47 (1975)

[Gob 73] A. Gobbi, et.al., Phys. Rev. C 7, 30 (1973)

[Gol 74] D.A. Goldberg, et.al., Phys. Rev. C 10, 1362 (1974)

[Gol 75] D.A. Goldberg, Phys. Lett. 55 B, 59 (1975)

[Gub 78] H.P. Gubler, et.al., Phys. Lett. 74 B, 202 (1978)

[Kön 77] R. Könnecke, et.al., in Proc. Int. Conf. on Resonances in Heavy-Ion Reactions, Hvar, (1977) p.109, Ed. N. Cindro

[Lee 77] S.Y. Lee and Y-D. Chan, Univ. of Wash.preprint RLO-1388-743 (1977)

[Lee 78] S.Y. Lee, Univ. Washington preprint (1978)

[Lip 78] R. Lipperheide, et.al., Contribution No. 30 to this conferene

[Löh 78] H. Löhner, et.al., Z. Physik A 286, 99 (1978)

[Lov 78] W.G. Love, Phys. Rev. C 17, 1876 (1978)

[McV 71] K.W. Mc Voy, Phys Rev. C 3, 1104 (1971)

[Mic 77] F. Michel and R. Vanderpoorten, Phys. Rev. C 16, 142 (1977)

[Pau 78] M. Paul, et.al., Phys. Rev. Letters 40, 1310 (1978)

[Sat 77] G.R. Satchler, Nucl. Phys. A 279, 493 (1977)

[Sel 78] T.P.F. Sellschop, et.al., Contribution No 32 to this conference

[Sha 74] D. Shapira, et.al., Phys. Rev. C 10, 1063 (1974)

[Shk 78] V. Shkolnik, et.al., Phys. Letts., 74 B, 195 (1978)

[Sie 77] R. Siemssen in Proc. Int. Conf. on Resonances in Heavy-Ion Reactions, Hvar, (1977), p 79, Ed. by N. Cindro

[Sto 72] R. Stock, et.al., Phys. ReV. C6 , 1226 (1972), Ed. R. Stock.

[Sto 72b] R. Stock, Proc. Symposium on Four Nucleon Correlations and Alpha Rotator Structure, Marburg (1972)

[Tak 77] N. Takigawa and S.Y. Lee, Nucl. Phys. A 292, 173 (1977)

[Tak 78] T. Takamesa and T. Tamura, Preprint, University of Texas (1978)

[Tak 78a] N. Takigawa, et.al., Phys. Letts. 76 B, 187 (1978)

[Tam 72] T. Tamura and H.H. Wolter, Phys. Rev. C 6, 1976 (1972)

[Tro 74] W. Trombik, et.al., Phys. Rev. C 9, 1813 (1974)

[Van 74] R. Vandenbosch, et.al., Phys. Rev. Letters 33, 842 (1974)

[Von 70] W. von Oertzen, Nucl. Phys. A 148, 529 (1970)

[Wie 76] R.M. Wieland, et.al., Phys. Rev. Letters 37, 1458 (1976)

[Wit 75] M. Wit, et.al., Phys. Rev. C 12, 1447 (1975)

Figure Captions

Fig 1. Elastic and inelastic scattering angular distributions for ^{40}Ca and ^{44}Ca. The full curves are folding model calculations. Dashed curves are P_L^2 L=13 (36.2 and 39.6 MeV), L=14 (42.6 MeV) and L=16 (49.5 MeV). From [Löh 78].

Fig 2. Excitation energy in the $\alpha + {}^{40}Ca$ system versus L(L+1), where L is extracted from a P_L^2 analysis of the back-angle enhancement . The dot-dash line shows the grazing angular momentum. The small dots at the side indicate energies for which data exist. From [Löh 78].

Fig 3. Measured cross sections for $^{16}O + {}^{28}Si$ [Cra 76] and predictions using a folded potential [Sat 77] or a shallow Woods-Saxon (E 18), [Cra 76].

Fig 4. Elastic scaltering of ^{16}O by ^{28}Si at E_{lab} = 55 MeV [Bra 77]. The dashed line was obtained using the E 18 potential [Cra 76] whereas the full line is a Regge-pole analysis [Bra 77].

Fig 5. Angular distributions for the elastic scattering of ^{12}C by ^{28}Si [Clo 78].

Fig 6. Excitation function for $^{16}O + {}^{28}Si$ at $175^o - 180^o$ [Bar 78]. The solid line is an optical model fit with a parity-dependent potential [Den 78], the broken line, without. The arrows denote for each the positions at which the real phase shift changes rapidly with energy.

Fig 7. Energies of rotational states in the $^{40}Ca + \alpha$ system [Fri 75]. a) The minima of the static potential. b) The position of resonances in a full dynamic calculation. The vertical bars indicate the calculated widths. c) The experimental values.

Fig 8. Excitation functions for $^{12}C + ^{28}Si$ elastic and inelastic scattering at $\theta=175^{o} - 180^{o}$. [Bar 78].

Fig 9. Schematic model for interpreting coexistance of broad and fine structures in excitation functions [Kön 77].

Fig 1o. $^{4o}Ca(\alpha,\alpha)$ ^{4o}Ca differential cross sections as a function of scattering angle at selected energies. The solid (broken) line corresponds to the best fit obtained using the folding (phenomenological) real potential. [Gub 78].

Fig 11. The normalization of the real folding potential, G_r, and the depth of the imaginary potential, V_{1o}, obtained in a fit to the data (see Fig 1o) at each bombarding energy. [Gub 78].

Fig 12. A comparison of empirical U_P [Mic 77] and double-folded U_F potentials [Lov 78] for $+ ^{4o}Ca$ scattering. M 3 Y and M 245 refer to different values of the nucleon-nucleon force.

Fig 13. a) The real and imaginary potentials deduced by Shkolnik et.al.[Shk 78] from a fit to the data shown in Fig 4.
b) corresponding graph for the E 18 potential of Cramer et al. From [Den 77].

Fig 14. The S-matrices for the different potentials shown in Fig 13. From [Den 77].

Fig 15. The real part of a potential (l=15) appropriate for 29 MeV scattering from ^{4o} ^{44}Ca. From [Bri 77].

Fig 16. Values of the S-matrix for the inner wave, η_I and the barrier wave η_B, for an absorption appropriate for ^{4o}Ca (W=16.6) and for ^{44}Ca (W=26.6). From [Bri 77].

Fig 17. The total S-matrix obtained by coherent summation of η_I and η_B shown in Fig 16. From [Bri 77].

Fig 18. Cross sections calculated for the inner wave alone, for the barrier wave alone, and for their sum. From [Bri 77].

Fig 19. With apologies to Charles Schultz (Permission requested).

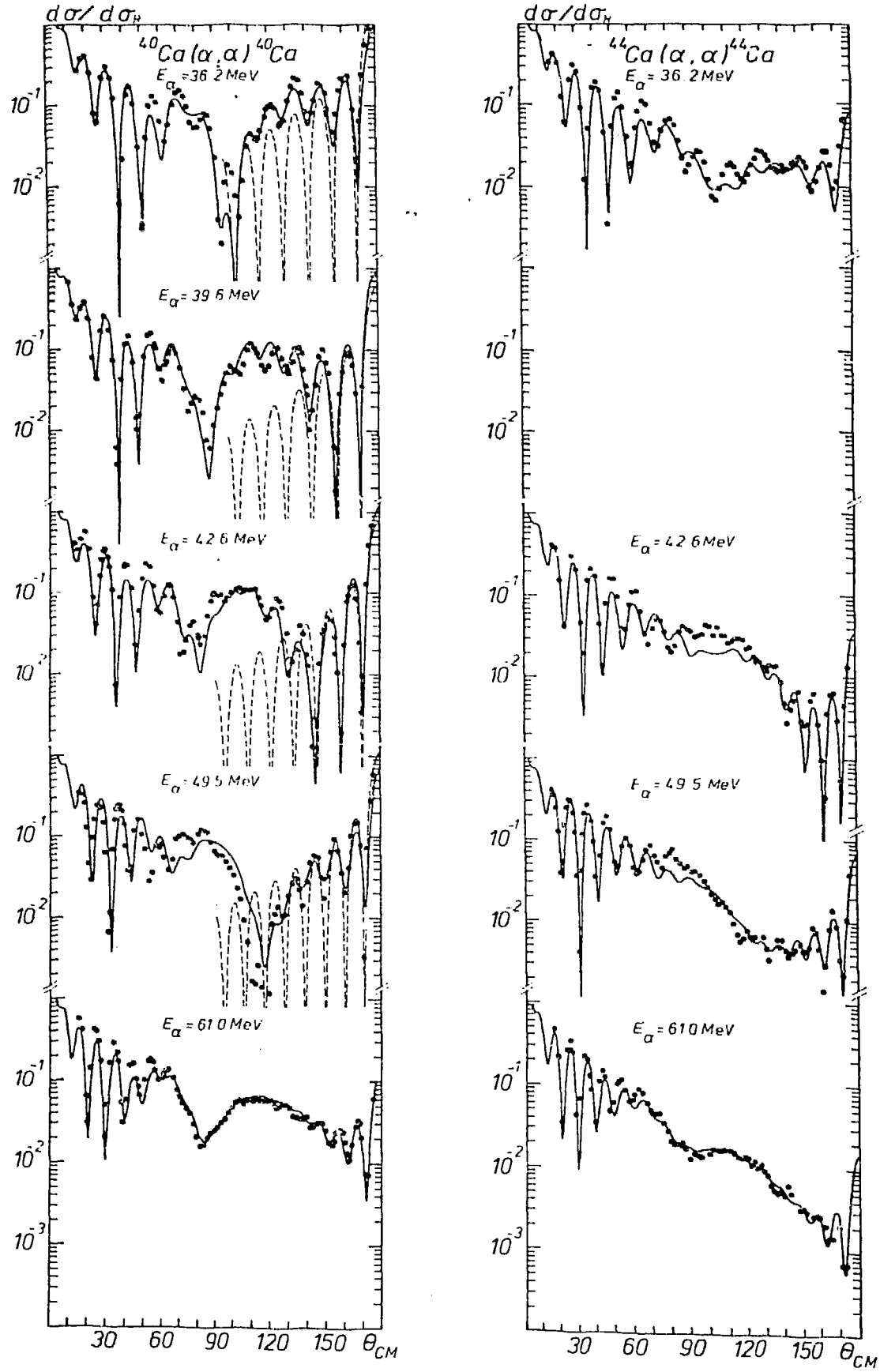
dσ/dσR
40Ca(α,α)40Ca
Eα=36.2MeV
Eα=39.6MeV
Eα=42.6MeV
Eα=49.5MeV
Eα=61.0MeV
44Ca(α,α)44Ca
Eα=36.2MeV
Eα=42.6MeV
Eα=49.5MeV
Eα=61.0MeV
10-1
10-2
10-3
30
60
90
120
150
θCM

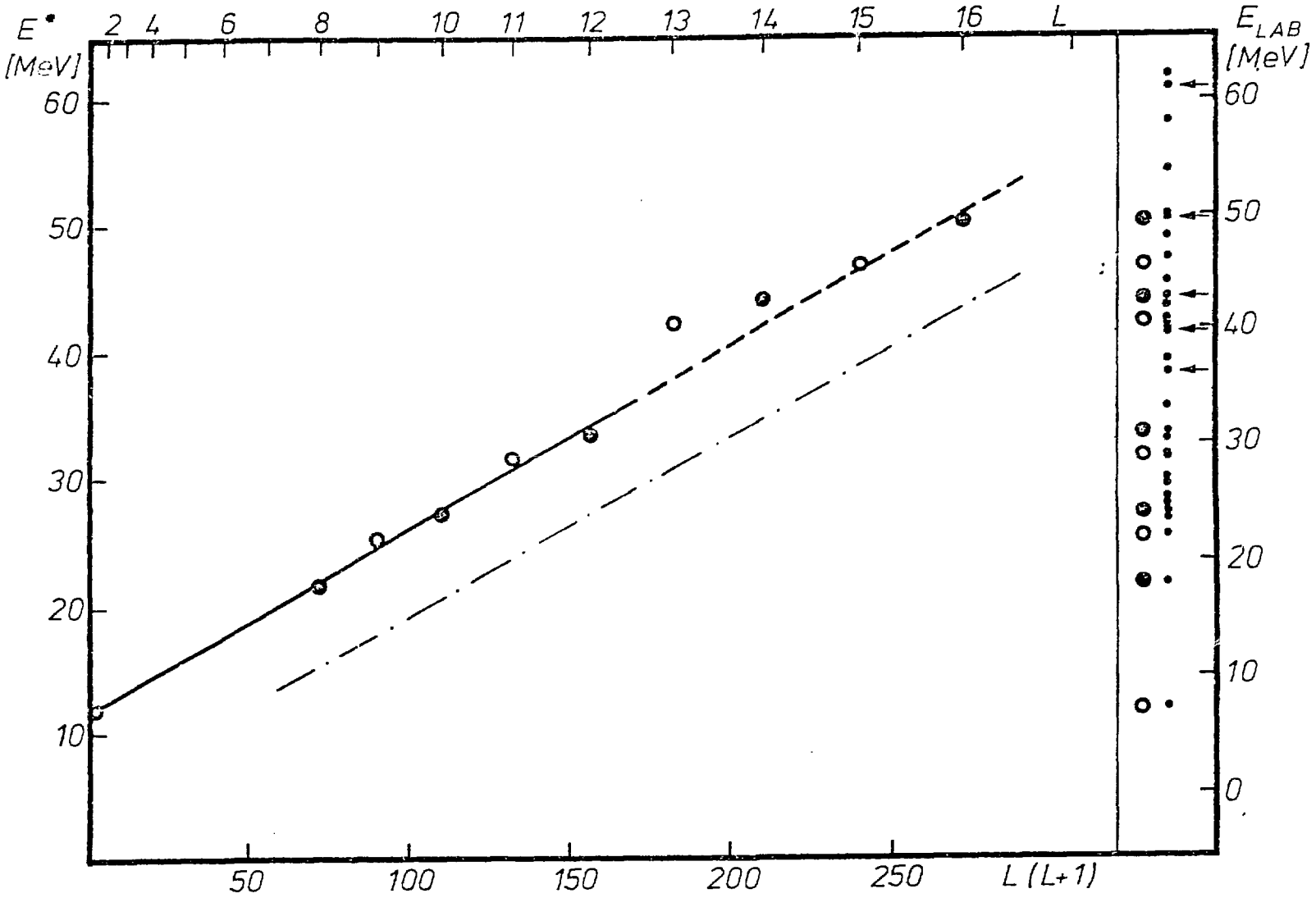
E*
[MeV]
2
4
6
8
10
11
12
13
14
15
16
L
60
50
40
30
20
10
50
100
150
200
250
L (L+1)
E_LAB
[MeV]
60
50
40
30
20
10
0

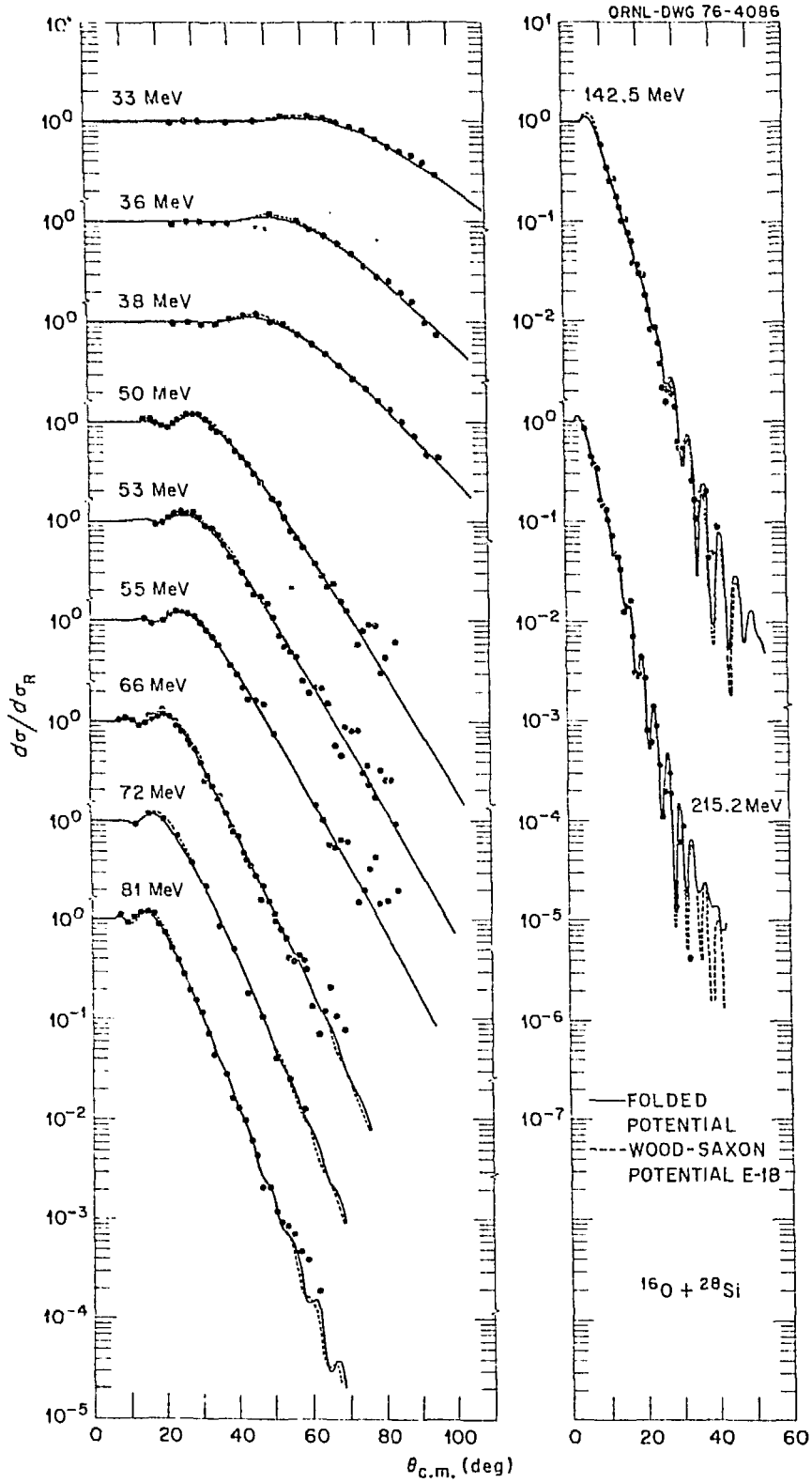
ORNL-DWG 76-4086
33 MeV
36 MeV
38 MeV
50 MeV
53 MeV
55 MeV
66 MeV
72 MeV
81 MeV
142.5 MeV
215.2 MeV
FOLDED POTENTIAL
WOOD-SAXON POTENTIAL E-18
$^{16}O + ^{28}Si$
$d\sigma/d\sigma_R$
$\theta_{c.m.}$ (deg)

Fig. 3

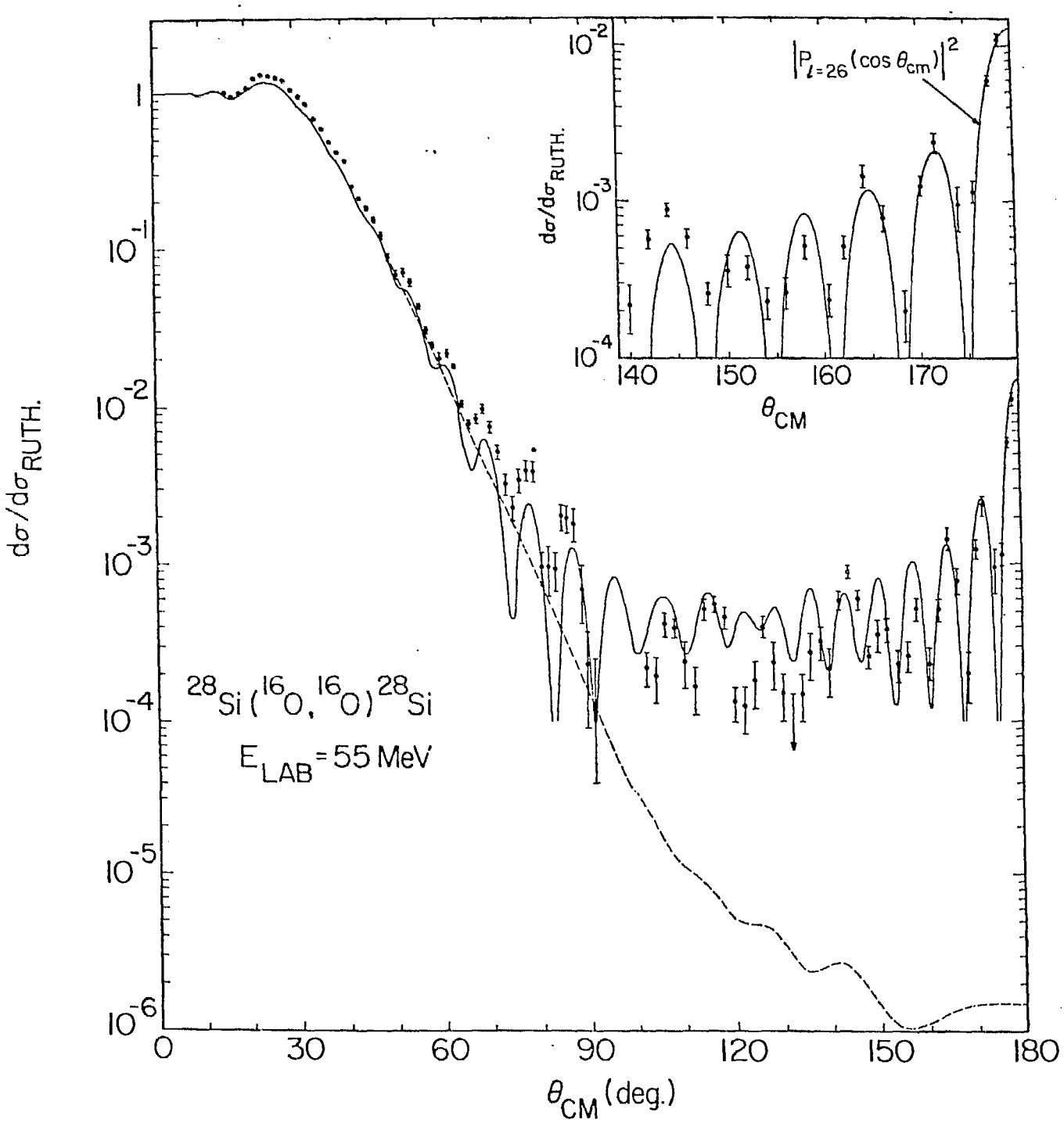
$^{28}Si(^{16}O,^{16}O)^{28}Si$
E_{LAB} = 55 MeV
$d\sigma/d\sigma_{RUTH.}$
θ_{CM} (deg.)
$|P_{l=26}(\cos\theta_{cm})|^2$
θ_{CM}

Fig. 4

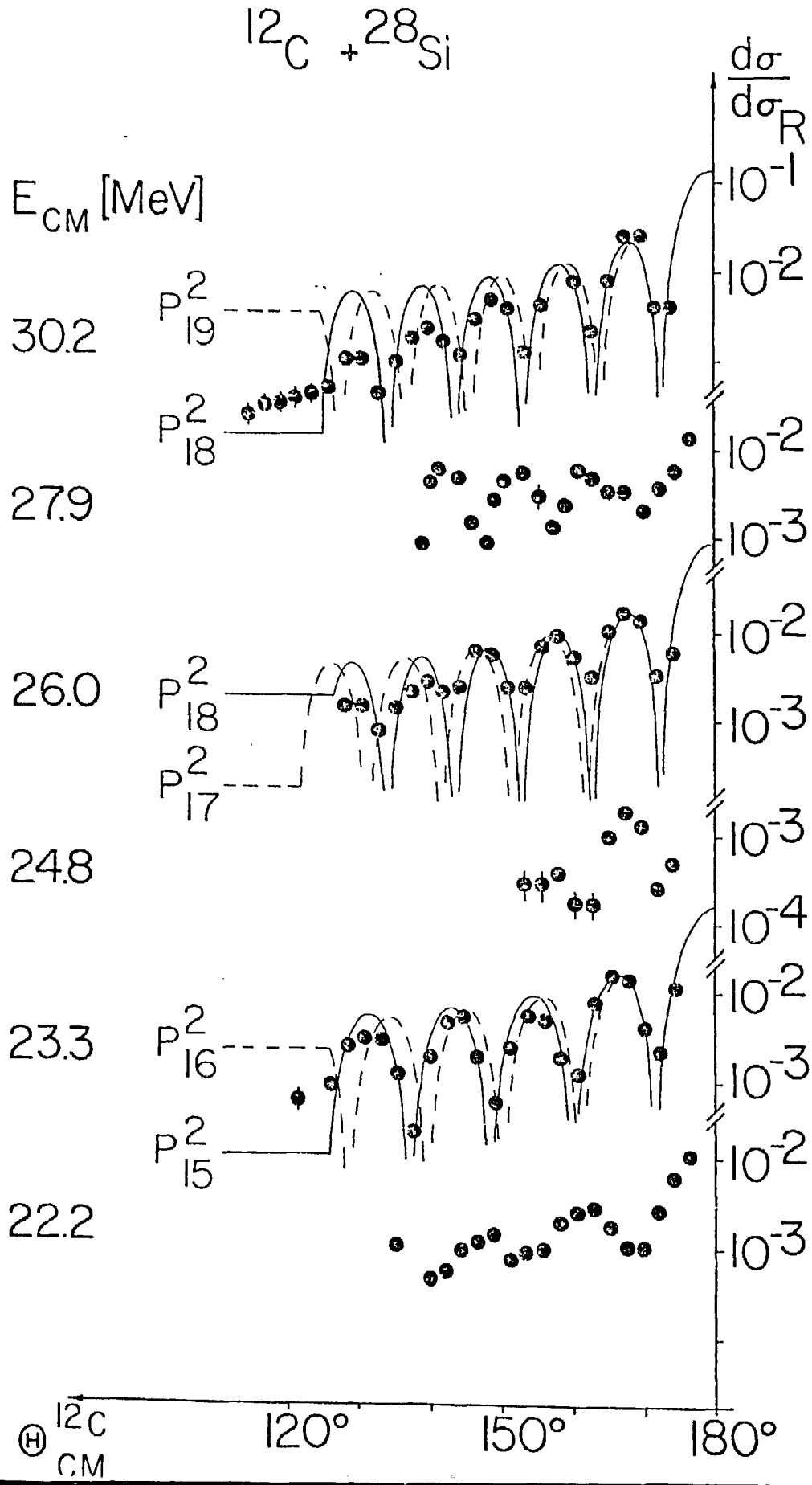
$^{12}C + ^{28}Si$
$\frac{d\sigma}{d\sigma_R}$
E_{CM} [MeV]
30.2
27.9
26.0
24.8
23.3
22.2
P^2_{19}
P^2_{18}
P^2_{18}
P^2_{17}
P^2_{16}
P^2_{15}
10^{-1}
10^{-2}
10^{-2}
10^{-3}
10^{-2}
10^{-3}
10^{-3}
10^{-4}
10^{-2}
10^{-3}
10^{-2}
10^{-3}
$\Theta_{^{12}C\,CM}$
120°
150°
180°

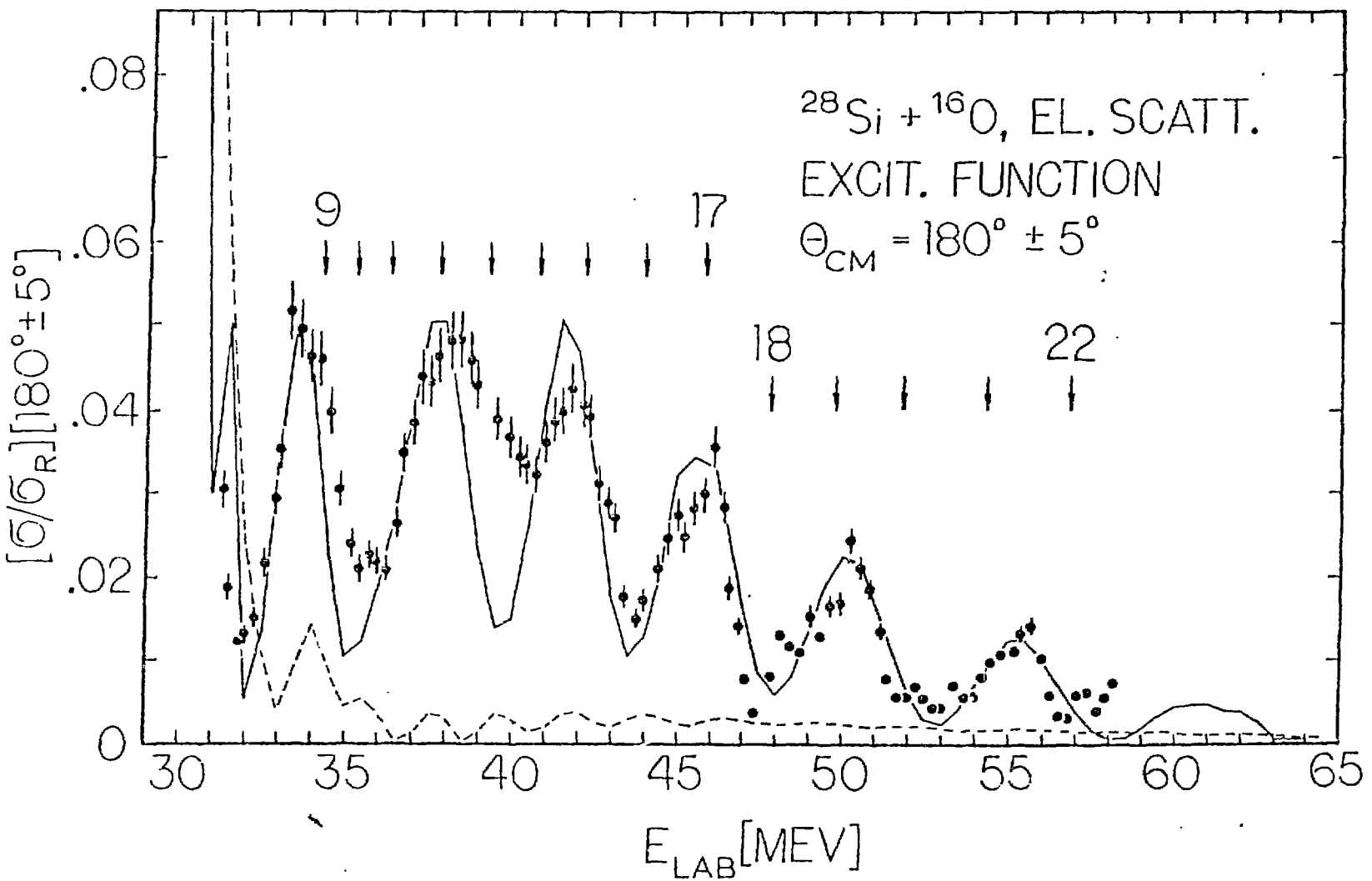
$^{28}Si + ^{16}O$, EL. SCATT.
EXCIT. FUNCTION
$\Theta_{CM} = 180° \pm 5°$
9
17
18
22
.08
.06
.04
.02
0
30
35
40
45
50
55
60
65
$[\sigma/\sigma_R][180° \pm 5°]$
E_{LAB}[MEV]

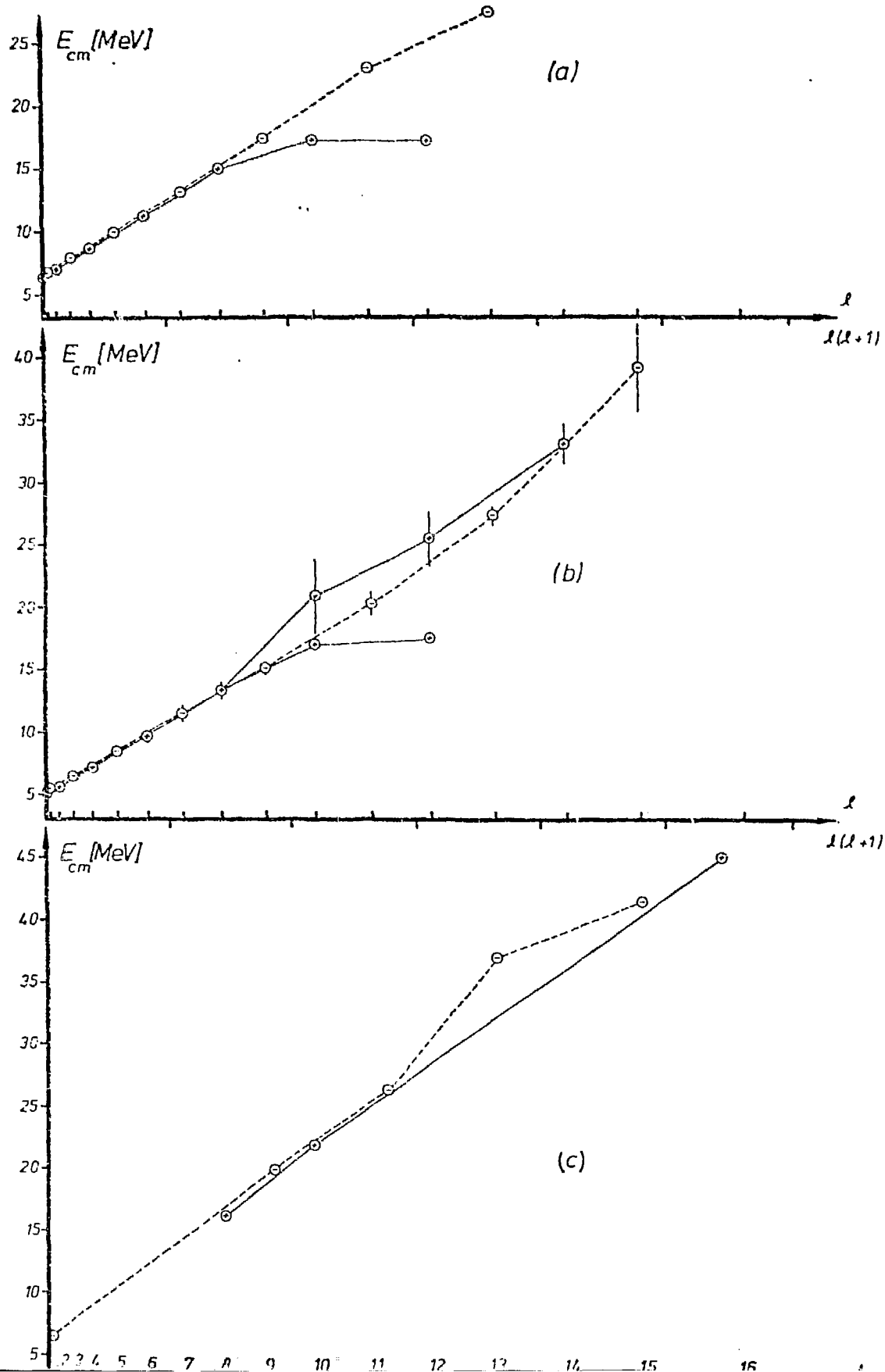
E_{cm} [MeV]
(a)
ℓ
$\ell(\ell+1)$
E_{cm} [MeV]
(b)
ℓ
$\ell(\ell+1)$
E_{cm} [MeV]
(c)

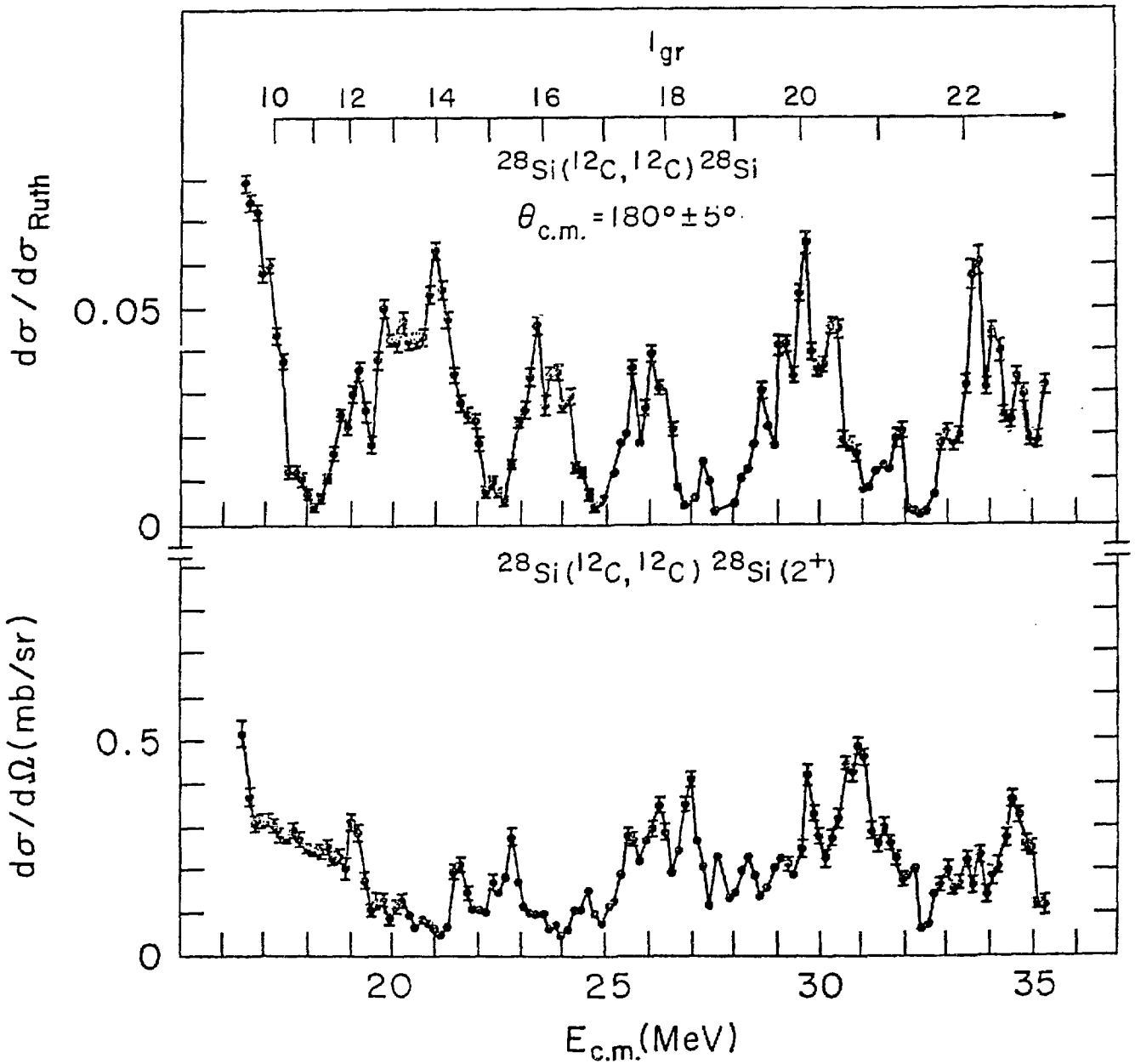
l_{gr}
10
12
14
16
18
20
22
$^{28}Si(^{12}C,^{12}C)^{28}Si$
$\theta_{c.m.} = 180° \pm 5°$
$d\sigma/d\sigma_{Ruth}$
0.05
0
$^{28}Si(^{12}C,^{12}C)^{28}Si(2^+)$
$d\sigma/d\Omega$ (mb/sr)
0.5
0
20
25
30
35
$E_{c.m.}$(MeV)

Fig. 8

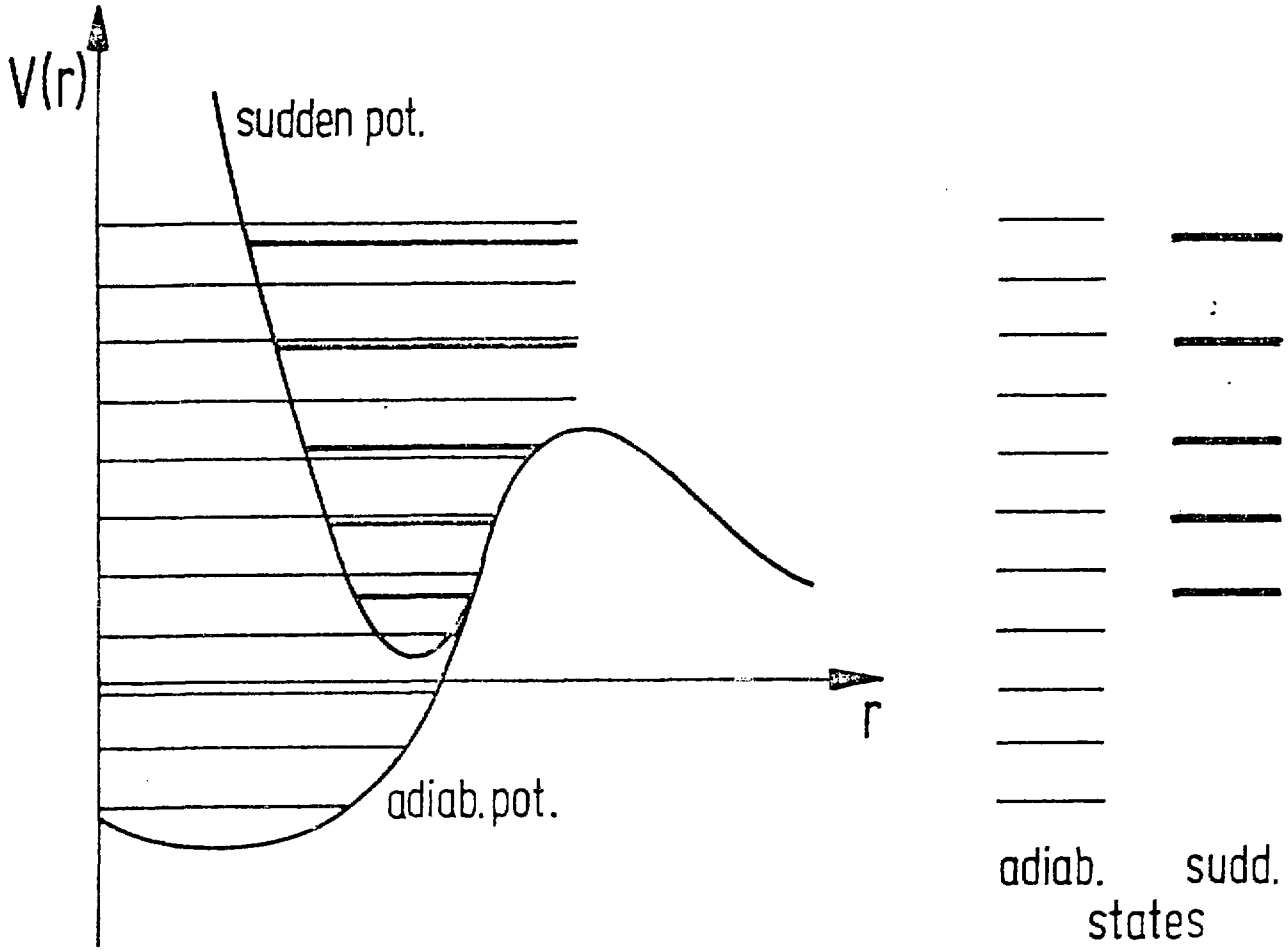

Coexistence Model

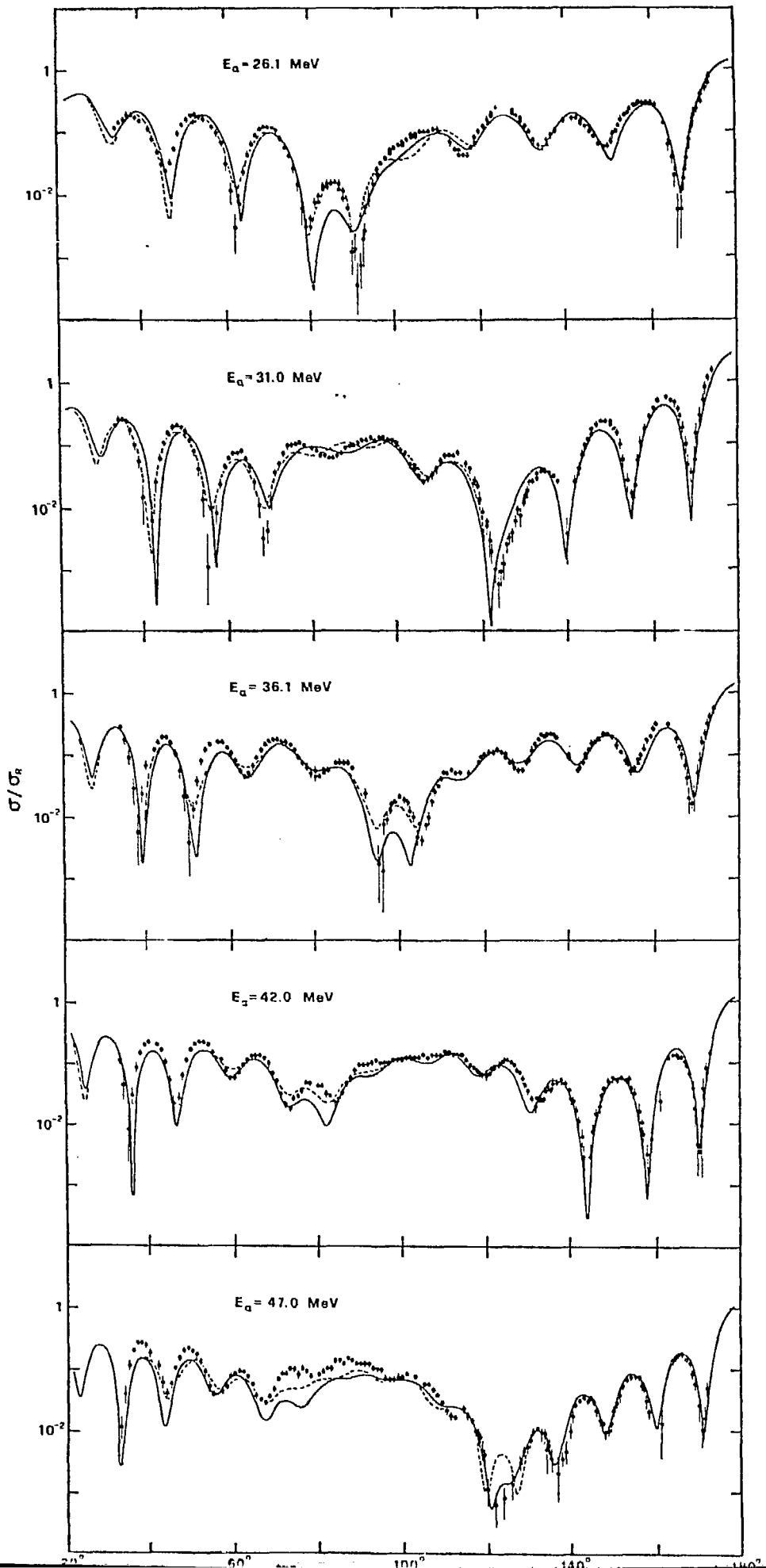
E_α = 26.1 MeV
E_α = 31.0 MeV
E_α = 36.1 MeV
E_α = 42.0 MeV
E_α = 47.0 MeV
σ/σ_R
1
10^{-2}
60°
100°
140°

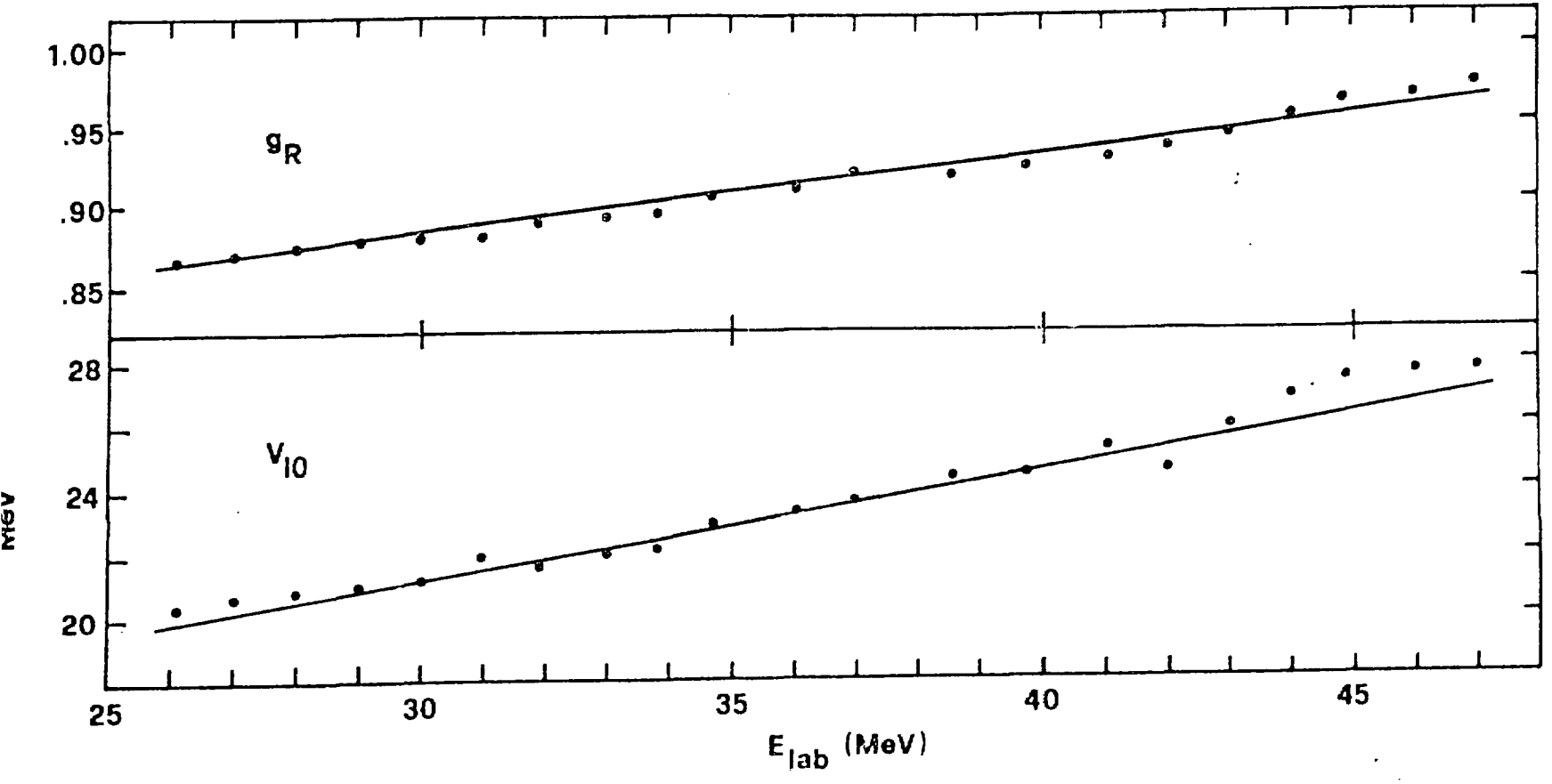

Fig. 11

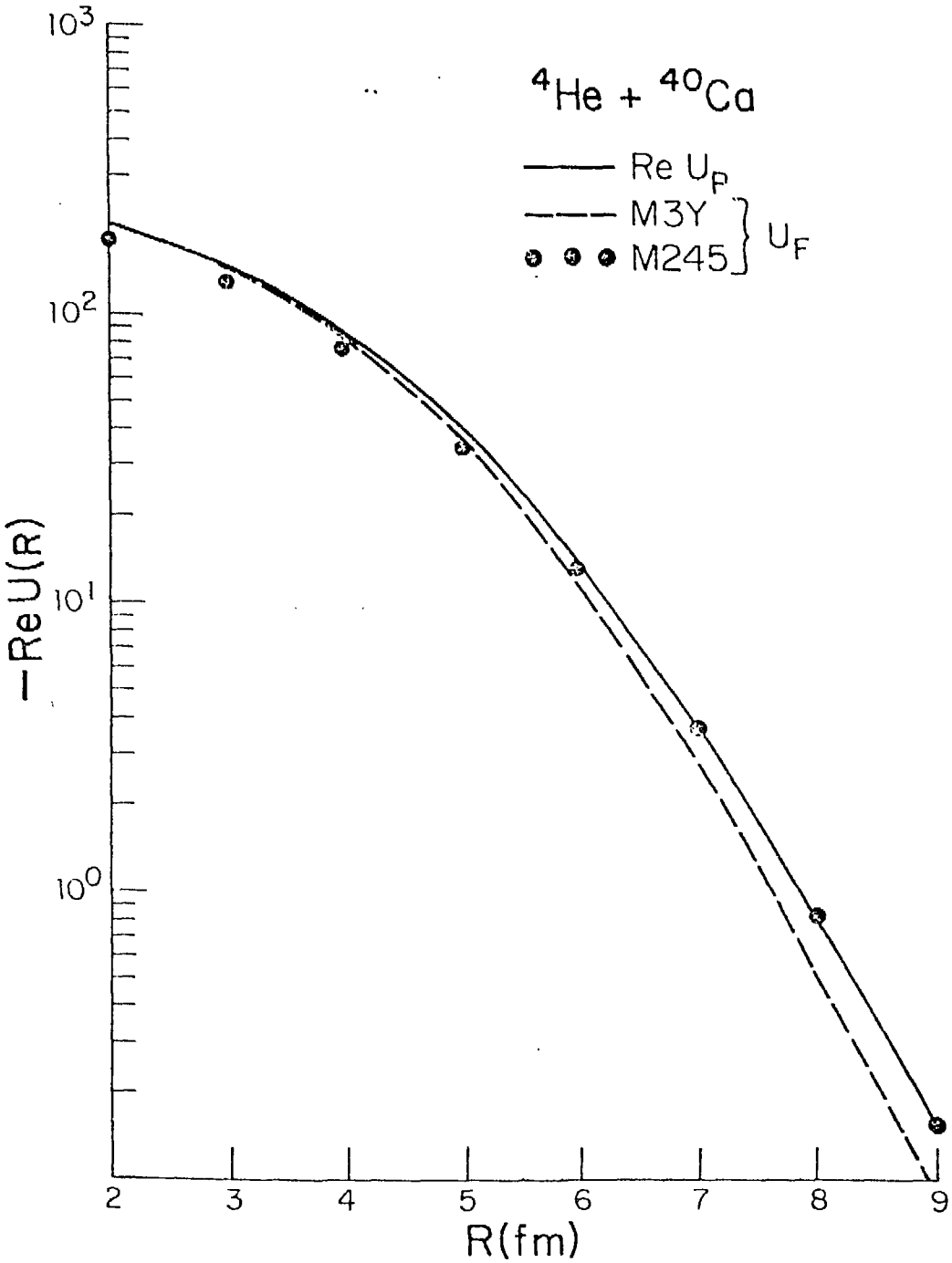

Fig. 12

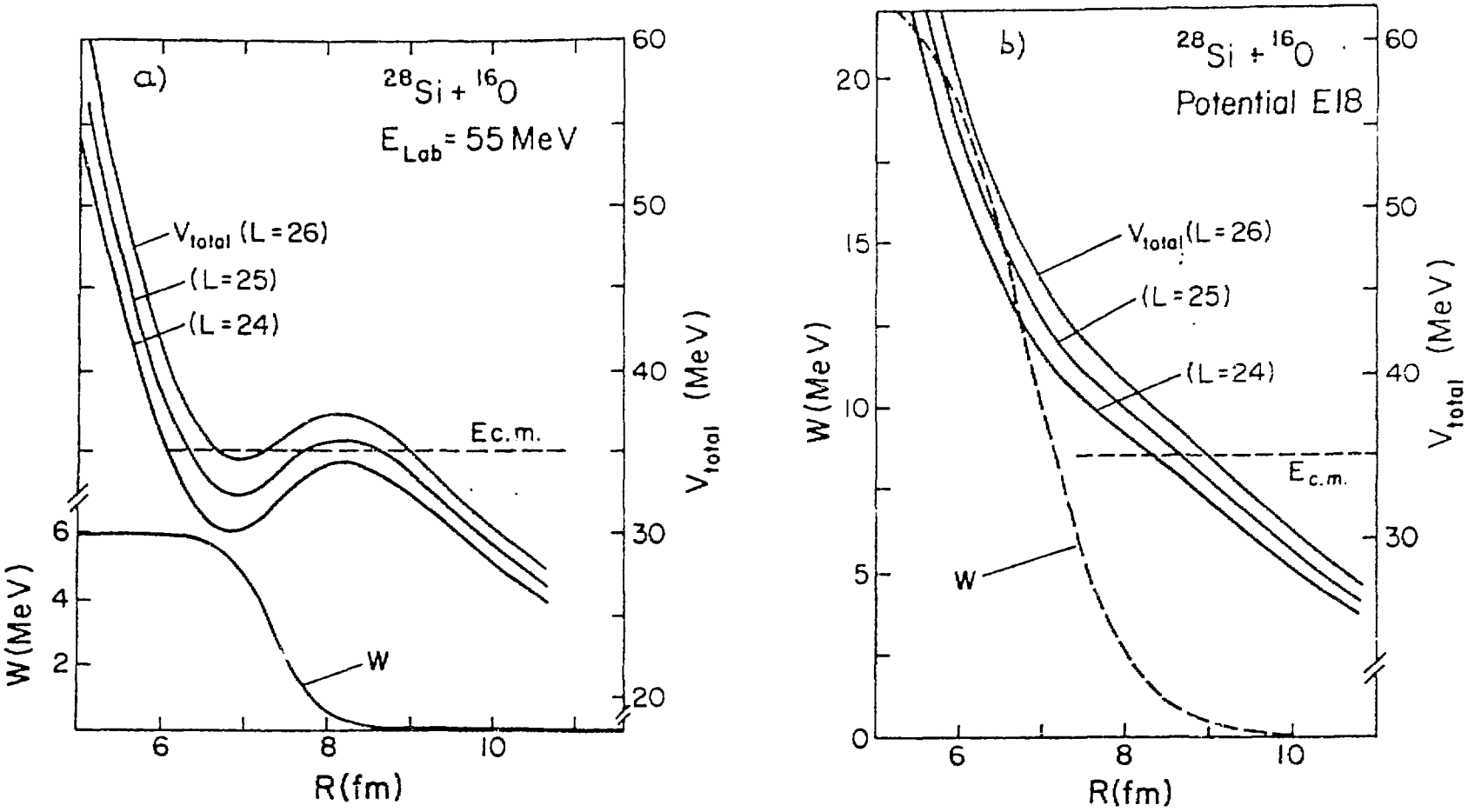
a)
$^{28}Si + ^{16}O$
E_{Lab} = 55 MeV
V_{total} (L=26)
(L=25)
(L=24)
Ec.m.
W
W(MeV)
V_{total} (MeV)
R(fm)
b)
$^{28}Si + ^{16}O$
Potential E18
V_{total}(L=26)
(L=25)
(L=24)
$E_{c.m.}$
W
W(MeV)
V_{total} (MeV)
R(fm)

Fig. 13

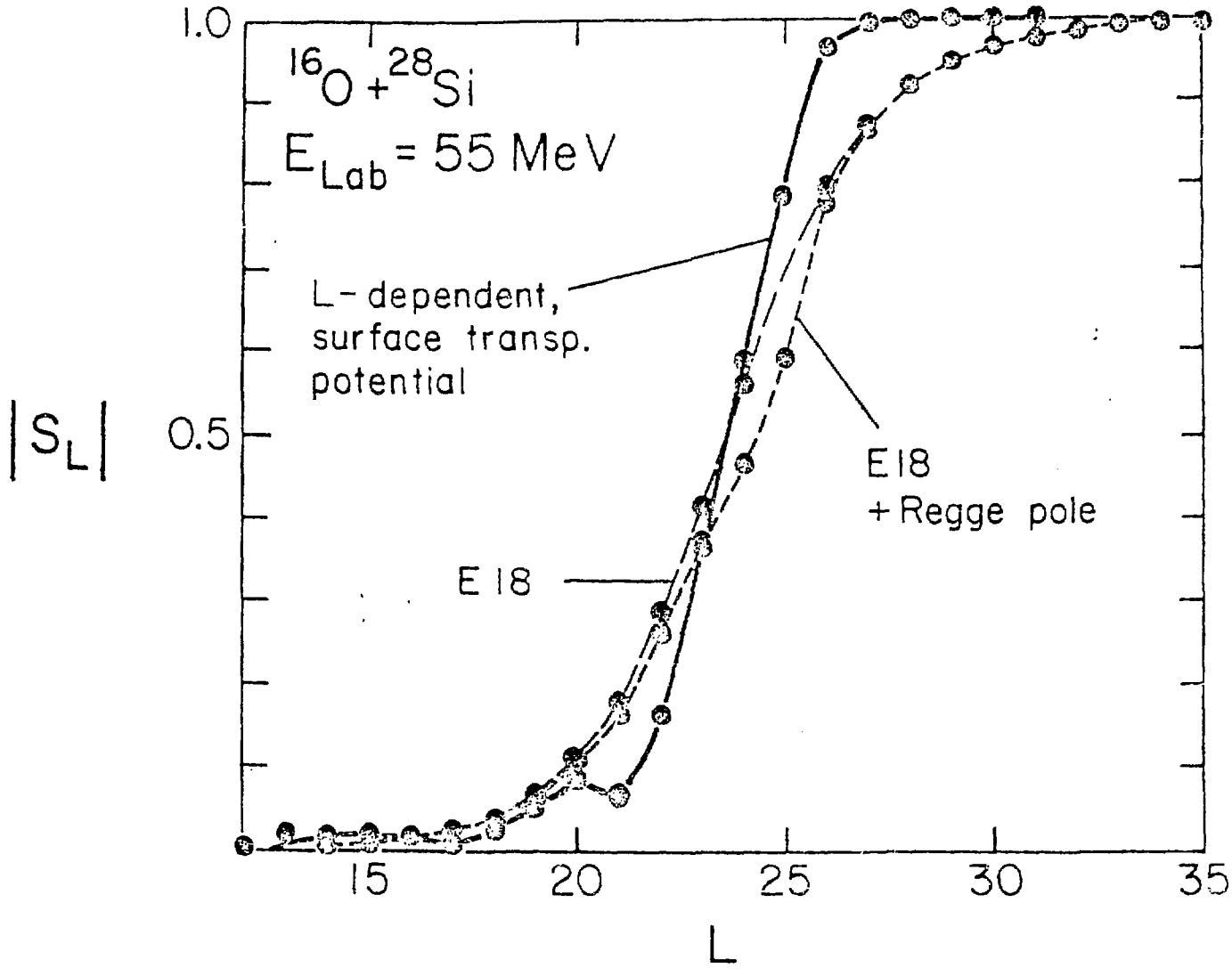
1.0
0.5
$|S_L|$
$^{16}O + ^{28}Si$
$E_{Lab} = 55$ MeV
L-dependent, surface transp. potential
E18 + Regge pole
E 18
15
20
25
30
35
L

Fig. 14

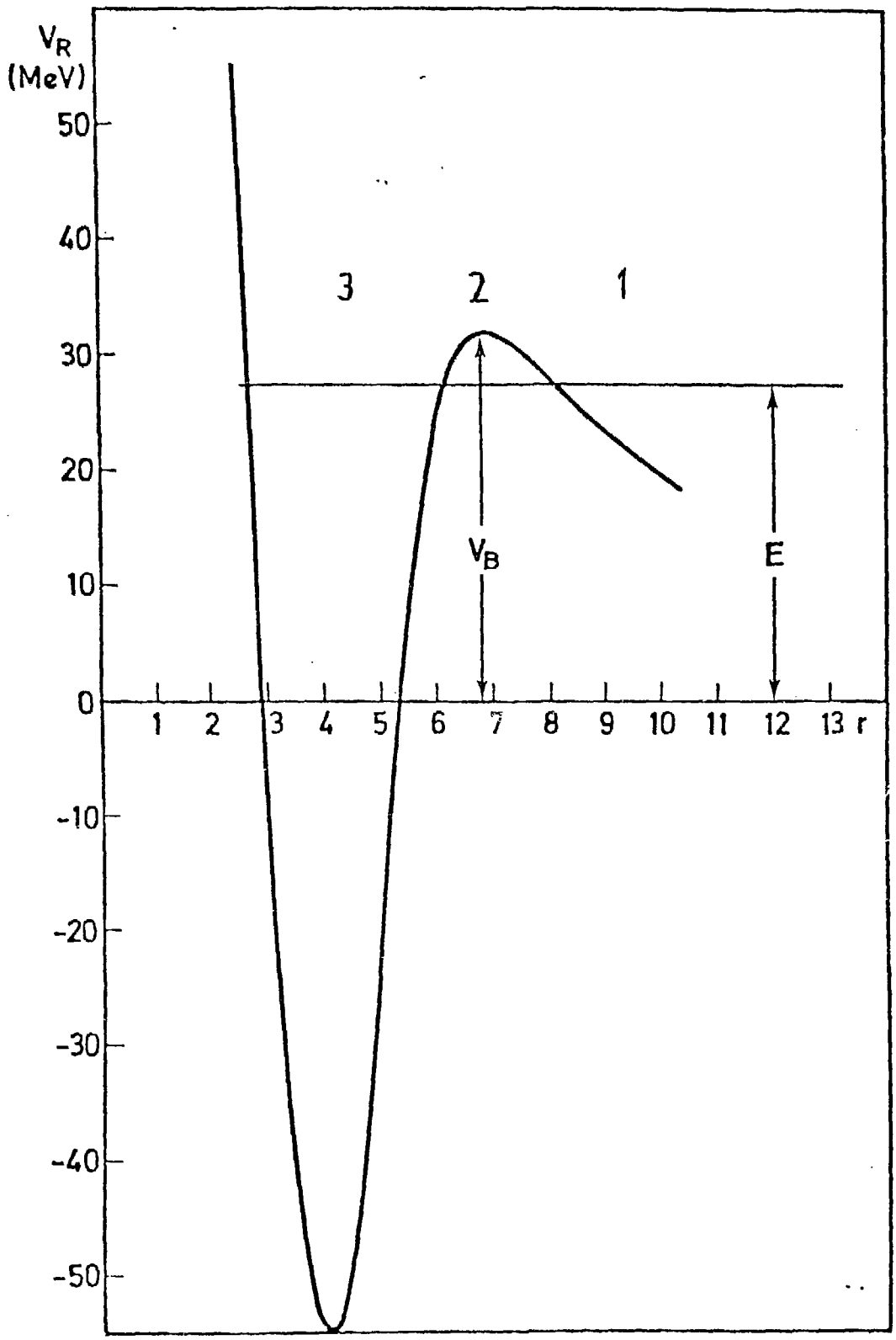
V_R
(MeV)
50
40
30
20
10
0
-10
-20
-30
-40
-50
3
2
1
V_B
E
1
2
3
4
5
6
7
8
9
10
11
12
13
r

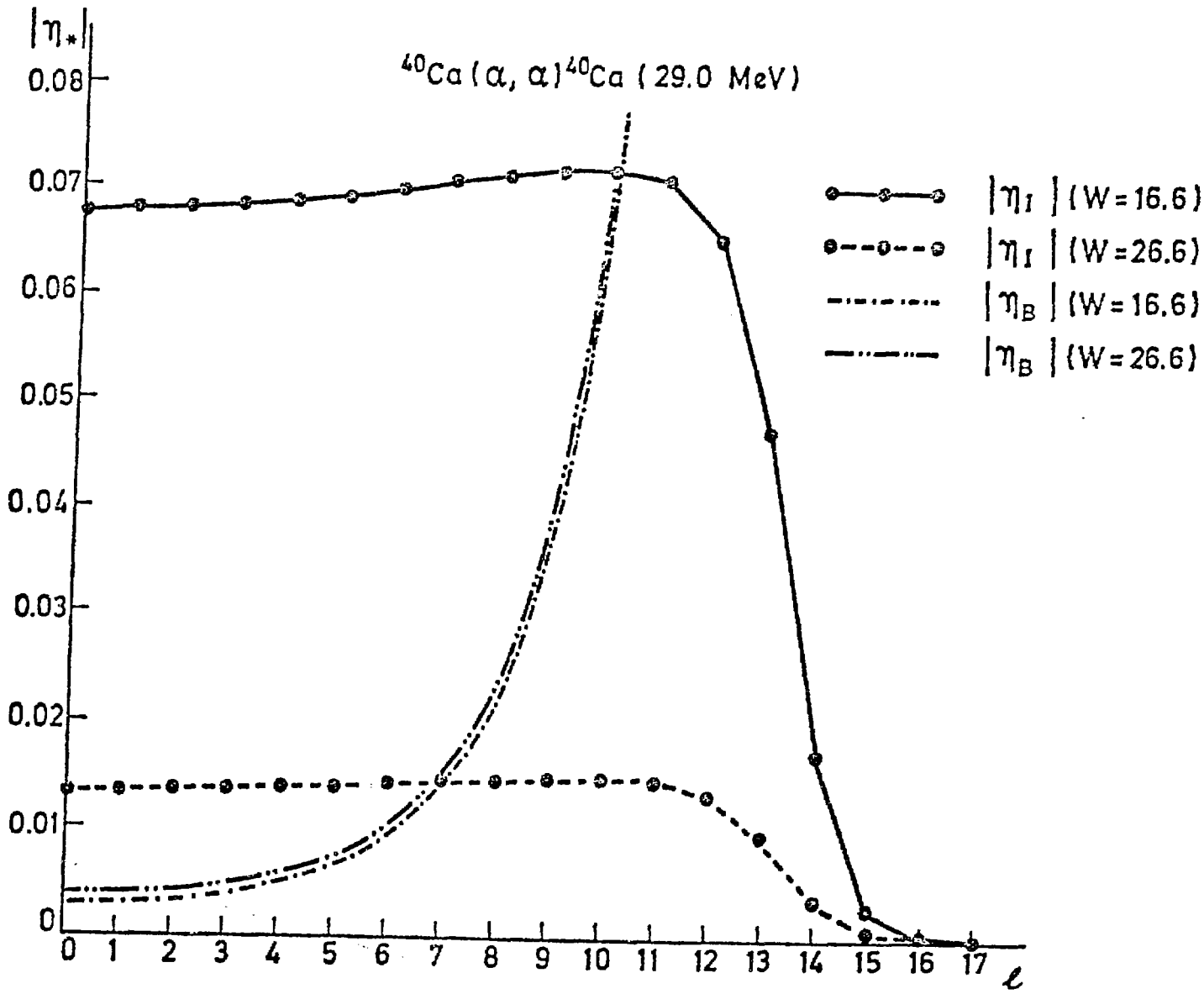
$|\eta_*|$
$^{40}Ca(\alpha,\alpha)^{40}Ca$ (29.0 MeV)
0.08
0.07
0.06
0.05
0.04
0.03
0.02
0.01
0
0 1 2 3 4 5 6 7 8 9 10 11 12 13 14 15 16 17
ℓ
$|\eta_I|$ (W = 16.6)
$|\eta_I|$ (W = 26.6)
$|\eta_B|$ (W = 16.6)
$|\eta_B|$ (W = 26.6)

Fig. 16

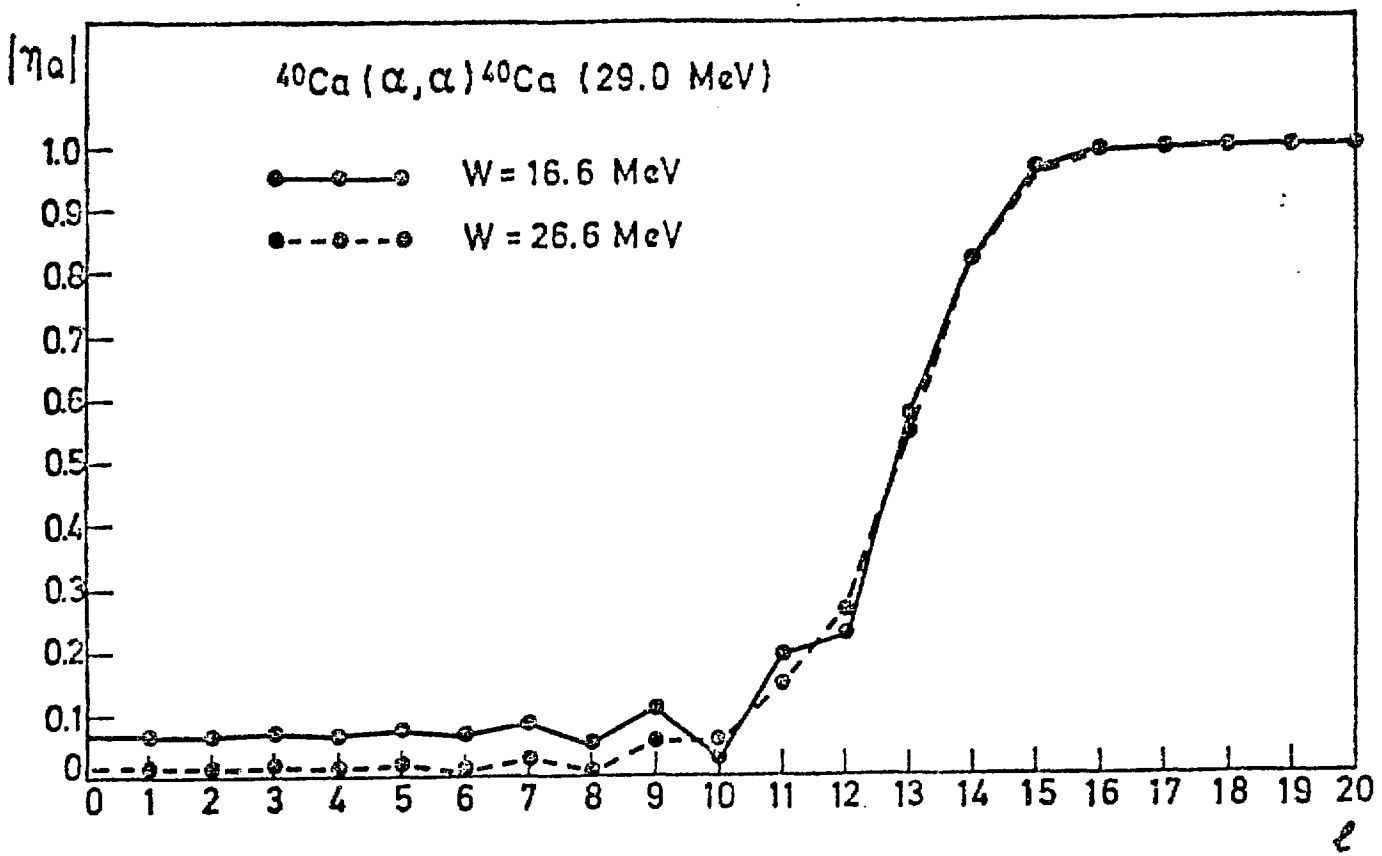
$|\eta_\alpha|$
$^{40}Ca(\alpha,\alpha)^{40}Ca$ (29.0 MeV)
W = 16.6 MeV
W = 26.6 MeV
1.0
0.9
0.8
0.7
0.6
0.5
0.4
0.3
0.2
0.1
0
0 1 2 3 4 5 6 7 8 9 10 11 12 13 14 15 16 17 18 19 20
ℓ

Fig. 17

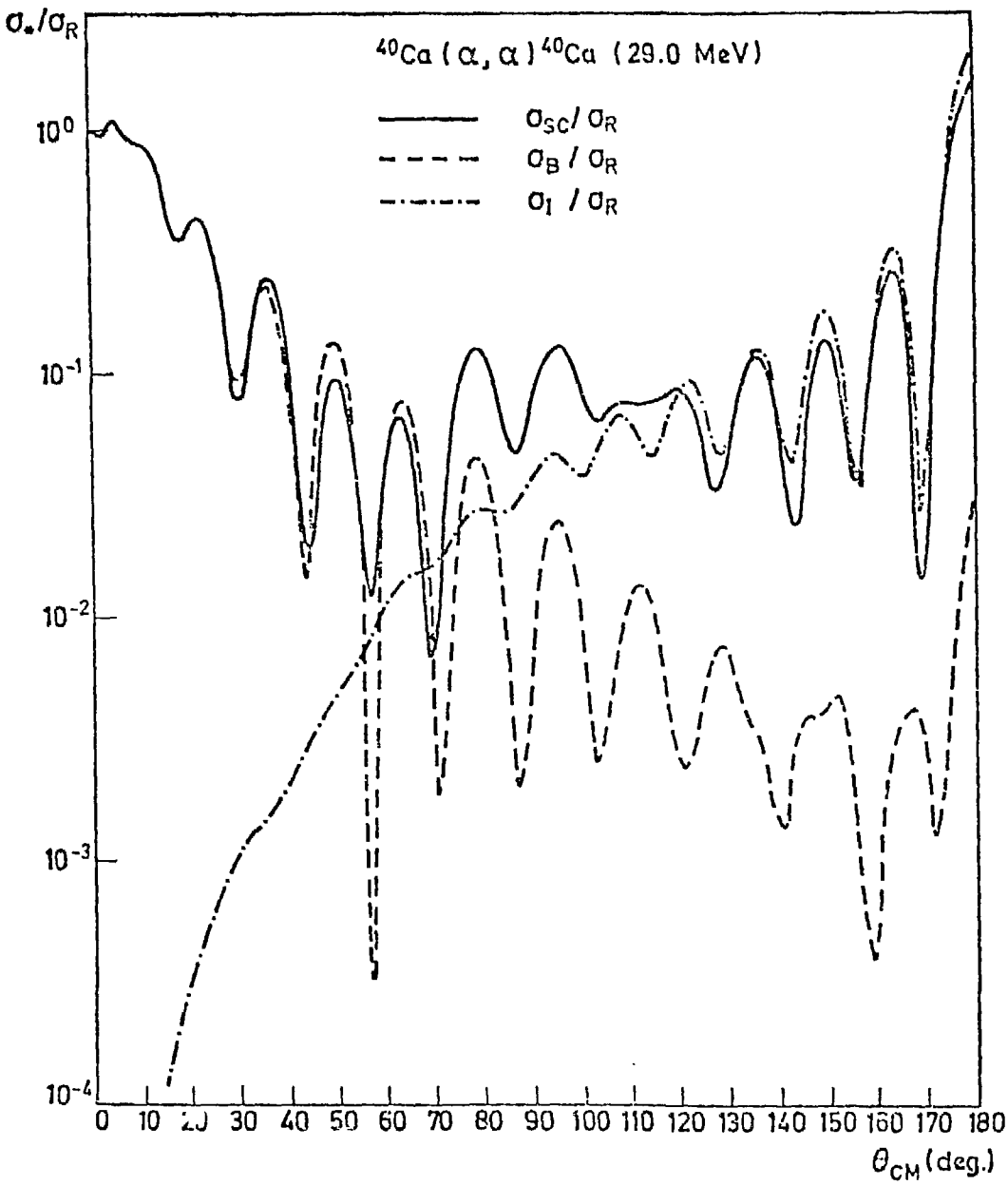
σ*/σR
40Ca (α, α) 40Ca (29.0 MeV)
σSC/ σR
σB / σR
σI / σR
10^0
10^-1
10^-2
10^-3
10^-4
0 10 20 30 40 50 60 70 80 90 100 110 120 130 140 150 160 170 180
θCM (deg.)

Fig. 18

I HAVE A LOT OF QUESTIONS ABOUT RESONANCES, AND I'M NOT GETTING ANY ANSWERS!
I WANT SOME REAL HONEST-TO-GOODNESS ANSWERS...
I DON'T WANT A LOT OF OPINIONS...I WANT ANSWERS!
WOULD TRUE OR FALSE BE ALL RIGHT?
SCHULZ